METEORITES

Their Record of Early Solar-System History

JOHN T. WASSON
University of California, Los Angeles

W. H. Freeman and Company

CHAPTER I

Meteorite Recovery, Fall Phenomena, Craters, and Orbits

Survey of the Solar System

The Moon and hundreds of artificial satellites are in orbit about the Earth; the Earth, the other planets, the asteroids, and the comets are in orbit about the Sun; and the Sun is in orbit about the center of the Milky Way galaxy. The basic equations describing the motions of these bodies are discussed in Appendix H.

Figure I-1 shows the orbits of the planets projected onto the ecliptic plane, the plane of the Earth's orbit; an inset shows the orbits of the inner planets at a larger scale. The planets are commonly divided into the inner, or terrestrial, planets (Mercury, Venus, Earth, and Mars) and the giant, or jovian, planets (Jupiter, Saturn, Uranus, and Neptune). Pluto does not seem to be a true planet, but rather a member of the set of smaller objects that accumulated to form Uranus and Neptune. Thousands of rocky bodies having radii in the range of 1 to 500 km[1] occupy orbits between those of Mars and Jupiter; a small fraction of these **asteroids**[2] are in other orbits, some of which cross the Earth's orbit. **Comets** are icy bodies that partially evaporate in the inner solar system to produce extended atmospheres; most comets are in highly elliptical orbits having long axes much greater than that of Neptune's orbit.

Most of the mass of the solar system is in the Sun, and most of the mass of the planetary system is in Jupiter. It is often handy to remember the fact that the mass of the Sun is ~1000 times[3] that of Jupiter, the mass of Jupiter ~1000 times that of the Earth, and the mass of the Earth ~1000 times that of the Ceres, which is by far the most massive asteroid. The properties of the planets, asteroids, and comets are discussed in more detail in Chapter IX.

Meteorites and Meteoroids

The solar system includes not only the planets, asteroids, and comets, but also solid objects ranging in size from bodies with radii of several kilometers

[1] See Appendix B for a list of the units used in this book.

[2] Definitions of specialized words are indicated by using **boldface** type for the word being defined.

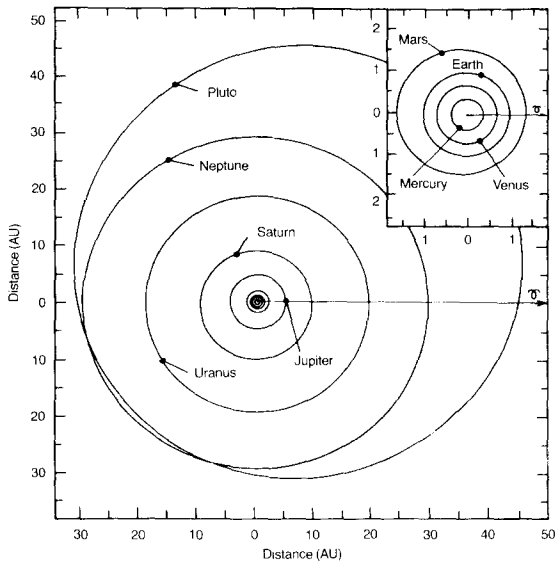

Figure I-1. Orbits of the planets projected onto the Sun–Earth (ecliptic) plane. Because the radii of the orbits of the planets increase exponentially with increasing distance from the Sun, it is not convenient to show them all on a single diagram. For this reason, the orbits of the inner planets are enlarged in the inset diagram. The orbits are nearly circular, except those of Mars and Pluto (which should no longer be classified as a planet). The arrow shows the direction from the Earth to the Sun at the time of the vernal equinox.

to submicroscopic dust. Some of these smaller objects are in **heliocentric** (Sun-centered, or planetlike) orbits that intersect that of the Earth. Such an object is called a **meteoroid** before it enters the Earth's atmosphere, a **meteor** when atmospheric friction makes it incandescent, and a **meteorite** if it is recovered. Meteorites recovered following observed falls are called **falls**; those recognized in the field that cannot be definitely associated with observed falls are called **finds.**

Meteorites having masses greater than 500 g fall at a rate of about one per 10^6 km^2 per year. Although about 150 fall on the land every year, only a few are recovered immediately following the fall. As a result, the chances are very small that an outdoors person such as a farmer will witness the fall of a subsequently recovered meteorite during a lifetime; the chances for an urban dweller are much smaller still.

As discussed in more detail in Chapter II, most meteorite falls are composed primarily of silicate minerals and are designated **stony meteorites**—or, where the meaning is clear from the context, simply "stones." Because they have a greater resistance to weathering and are more readily recognized in the field, meteorites composed largely of Fe–Ni metal are especially common among finds. These meteorites are designated **iron meteorites**, or simply "irons."

The Beginnings of Meteorite Study

Meteorite falls have been witnessed throughout human history. Iron meteorites were an important raw material to primitive peoples. In some cases, the heavenly source of this iron was recognized, as evidenced by etymological relationships.

Figure I-2 is a charming woodcut showing the fall of a meteorite in Ensisheim, Alsace, in 1492—a year well known to school children in the

Figure I-2. Woodcut depicting the fall of the Ensisheim LL chondrite on 7 November 1492. A literal translation of the German caption (by Sebastian Brant) is "of the thunder-stone (that) fell in xcii (92) year outside of Ensisheim." This meteorite, which is preserved in the city hall of Ensisheim, Alsace, is the oldest recorded fall from which material is still available.

Americas. In the original broadsheet, the major German author Sebastian Brant provided a verse description of the fall in Latin and German. The verse suggests that the Austrian king, Maximilian, won a battle against the Burgundians because the latter were terrified by the extraterrestrial fireworks above their heads. This meteorite was clearly recognized to have fallen from the sky.

However, during the eighteenth century (the "age of enlightenment"), scientists became convinced that reports of rocks from the sky were but the fantasies of peasants. Perhaps the situation arose because these learned men had never witnessed a meteorite fall, perhaps more so because their attempts to eliminate superstition led them to a general skepticism regarding the testimony of peasants and other inhabitants of rural places. In any case, it was possible for P. Bertholon to comment regarding the 1790 fall of a meteorite at Barbotan, France, "how sad it is that the entire municipality enters folk tales upon the official record." A. Stutz in 1790, in describing the fall of an iron meteorite near Hraschina, Croatia (Yugoslavia), noted "the straightforward manner with which everything is accounted, the agreement among the witnesses who had no grounds to agree so completely regarding a lie," but then concluded that "in our times it would be unforgivable to hold such tales to be probable." It has been widely quoted that, on hearing of the description of a meteorite fall at Weston, Connecticut, on 14 December 1807, Thomas Jefferson said, "It is easier to believe that two Yankee professors would lie, than that stones would fall from heaven." However, recent searches have failed to locate the source of this reputed quotation, and there is growing doubt that Jefferson actually made the statement. A skeptical but much more balanced statement, however, is found in Jefferson's letter to Daniel Solomon on 15 February 1808: "its [the Weston stone's] descent from the atmosphere presents so much difficulty as to require careful examination," but "we certainly are not to deny whatever we cannot account for," and "the actual fact . . . is the thing to be established."

The first clear and detailed exposition of the extraterrestrial nature of meteorites is found in a small book published by E. F. F. Chladni in 1794. Chladni not only showed that there was good factual support for the conclusion that bright fireballs often drop meteorites, but he also gave well-reasoned arguments for believing that certain large masses of iron are prehistoric meteorites. Soon after the distribution of his book, Chladni's ideas were supported by the publication of several reports of meteorite falls and by the discovery of the first two asteroids in 1801 and 1802. The fraction of the scientific community that held meteorites to be extraterrestrial, although minor, was clearly increasing.

It is commonly stated that the turning point occurred in 1803, when J. B. Biot, a young member of the Académie Française, investigated and strongly endorsed the correctness of reports that a shower of meteoritic stones had fallen from the sky at L'Aigle, France. In fact, the tide had started to turn a few years earlier. Although a few ingenious persons still hypothesized that meteorites are atmospheric condensations, these ideas faded during the following decades.

Fall Phenomena

The fall of a meteorite is typically a spectacular event. The meteoroid enters the atmosphere with a velocity of about 20 km $\cdot$ s^{-1}. At an altitude of about 100 km, atmospheric density is great enough to produce a significant amount of frictional drag. The kinetic energy lost in the deceleration of the meteoroid is converted primarily to heat and light. The brightness of the fireball is commonly great enough to be seen in daylight. Nighttime fireballs that reach the earth as meteorites are in most cases brighter than the full Moon.

Heating by the impacting air molecules melts the surface of the meteoroid. Selective erosion produces attractive hills and valleys called **regmaglypts**, particularly on iron meteorites. If a meteoroid maintains a fixed orientation during atmospheric passage, the regmaglypts on the leading surface become much deeper than those on the trailing surface. The iron from Cabin Creek, Arkansas, is the classic example of an oriented meteorite (Figure I-3). By the time the meteoroid reaches terminal velocity (a nearly constant velocity of $\sim$0.3 km $\cdot$ s^{-1} at which the deceleration by drag is approximately balanced by the acceleration by gravity), frictional heating is no longer sufficient to produce melting, and the final melt has congealed to form a fusion crust. Because heat conduction is a slow process, the interiors of meteoroids remain cold even when their surfaces are molten. Significant thermal effects usually extend inward a few centimeters in the efficiently conducting irons, but only several millimeters in the poorly conducting stones. The heat-altered zone of an iron-meteorite fall is readily recognized on a polished surface (Figure I-4).

The meteoroid is subjected to severe stresses during the deceleration to subsonic speeds from velocities many times supersonic. If it consists of **friable** (easily crumbled) material, it will disintegrate into individual grains and not penetrate as a rock-sized body to the Earth's surface. Even if it is tough, the stresses generally break up stones larger than several kilograms or irons larger than several tens of kilograms, resulting in a meteorite shower. The fracturing commonly occurs along preexisting cracks produced by impacts with other space debris prior to capture by the Earth. The shower of meteorites results in a **strewn field**, a set of meteorite fragments scattered over a certain geographic region that is typically elliptical in

Figure I-3. The two sides of the Cabin Creek, Arkansas, IIIAB iron are strikingly different, apparently because the meteoroid remained in a fixed orientation during atmospheric passage, with the face shown above leading and that on page 7 trailing. The total height is 44 cm. A meteoritic mass that was worshiped

in Ephesus is described in the biblical Acts of the Apostles. It seems likely that the interpretation of this meteorite as an Earth Goddess was prompted by a benippled appearance similar to Cabin Creek's dimpled leading side. (Photo from G. Kurat, Naturhistorisches Museum, Vienna)

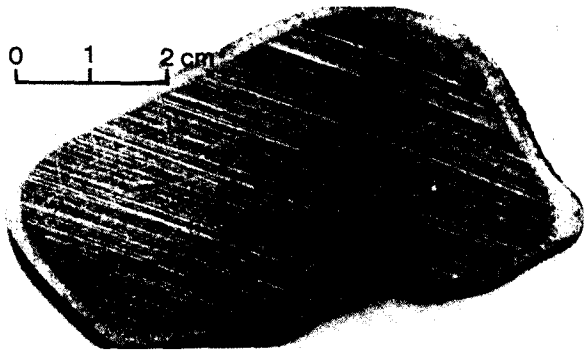

Figure I-4. A slice through the Avce, Yugoslavia, IIAB iron, an observed fall. The polished and etched surface of this hexahedrite is crossed by three sets of Neumann lines (shock-produced crystallographic twins) having different orientations. Frictional heating during atmospheric deceleration has produced a heat-altered zone free of Neumann lines around the edge of the section. (Photo from V. F. Buchwald, *Iron Meteorites*, University of California Press, 1975)

shape (Figure I-5). Because of their lower surface-to-mass ratios, larger stones travel farther than smaller stones along the "great circle" projection of the trajectory along the Earth's surface. The deceleration of the meteoroid also generates sonic booms. These thunderlike noises are heard chiefly by persons directly below the trajectory.

If they remain intact, the largest meteoroids are never fully decelerated to terminal velocity in the air; they retain some fraction of their preatmospheric velocity v_∞ at impact with the solid Earth. Figure I-6 shows the approximate theoretical relationship between the relative velocity v/v_∞ and a parameter K defined as

$$K = \frac{0.7D}{r\rho \sin \theta}$$

where D is the drag coefficient (which can take on values between 0 and 1), r is the radius in cm, ρ is the density in g · cm^{-3}, and θ is the atmospheric entry angle between the meteoroid's trajectory and the Earth's surface. For

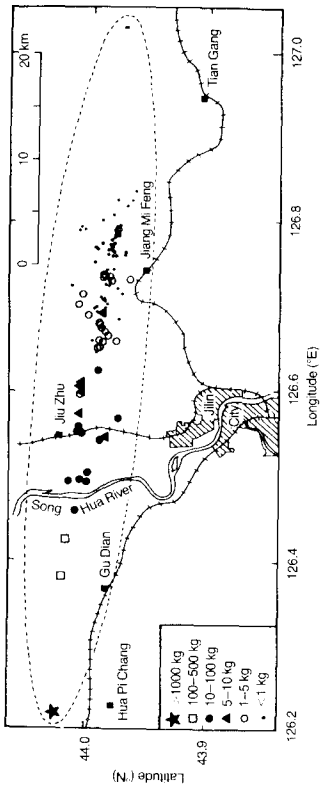

Figure I-5. Distribution of fragments from the shower of H chondrites near Jilin City, Jilin Province, China, on 8 March 1976. The meteoroid's direction of flight was toward the west. After disintegration in the atmosphere, the larger the fragment, the farther it traveled before striking the Earth. The resulting dispersion ellipse is typical of meteorite showers.

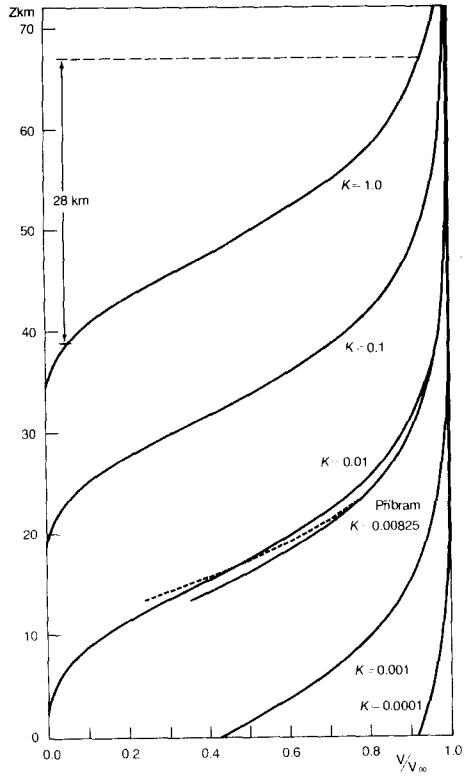

Figure I-6. Theoretical curves predicting the ratio of the velocity v of a meteoroid relative to the velocity v_∞ that it had immediately before striking the atmosphere, as a function of the altitude z and a parameter K that is inversely proportional to both radius and density. The dashed curve shows that the photographically determined path of the Přibram H5 chondrite is approximately matched by the appropriate $K = 0.00825$ curve. (From V. F. Buchwald, *Iron Meteorites*. University of California Press, 1975)

example, a 4-ton meteorite with a drag coefficient of 0.5 entering vertically ($\theta = 90°$) would follow the $K = 0.0001$ curve and strike the Earth's surface with about 92 percent of its preatmospheric velocity. When a meteoroid strikes the Earth, it makes a hole. The typical small meteorite falling onto soil at a subsonic terminal velocity produces a pit having a volume comparable to or somewhat larger than that of the meteorite. The whole or fragmented meteorite can be recovered from such a pit.

Craters and Other Phenomena Produced by Large Meteoroids

A meteoroid that impacts the surface with nearly its preatmospheric velocity produces an explosion; during such a **hypervelocity** impact, the solid matter splashes like a fluid, and a crater much larger than the meteoroid is excavated. At an impact velocity of 20 km · s^{-1}, the radius of the crater is ~10 times and the volume nearly 1000 times that of the meteoroid. The projectile is almost entirely vaporized on impact.

The best-preserved hypervelocity crater is Meteor Crater in northern Arizona, about 30 km west of Winslow (Figure I-7). Its diameter is approximately 1200 m. A few tens of tons of iron meteorite fragments have been recovered from the projectile, whose mass was roughly 4×10^{12} g prior to

Figure I-7. An IAB iron meteorite with a radius of about 50 m created Meteor Crater in the Coconino Sandstone of Northern Arizona ~25,000 to ~50,000 years ago. The squarish outline results from preferred fracturing along roughly perpendicular zones of weakness; most craters are more circular. The mean diameter is ~1200 m. The iron meteorites associated with the crater are named after the sinuous Canyon Diablo, which crosses the upper part of the photo. (Photo by D. J. Roddy, U.S. Geological Survey)

Table I-1
Meteorites found near hypervelocity explosion craters

Meteorite	Group	Crater diameter (m)	Estimated age (kyr)
Boxhole, Northern Terr., Australia	IIIAB	160	5
Canyon Diablo, Arizona, U.S.A.	IAB	1200	20–50
Henbury, Northern Terr., Australia	IIIAB	180	<5
Kaalijarv, Estonia	IAB	100	5
Monturaqui, Atacama, Chile	IAB	370	>100
Odessa, Texas, U.S.A.	IAB	160	50
Wabar, Saudi Arabia	IIIAB	100	<5
Wolf Creek, West. Aust., Australia	IIIAB	840	>100

Source: J. T. Wasson, *Meteorites*, Springer Verlag, 1974.

impact. Recognizable meteoritic debris has been found associated with eight hypervelocity craters. In each case, the projectile belonged to one of the two largest groups of iron meteorites (Table I-1). The absence of craters produced by stones partly reflects the fact that stones weather faster than irons, but it appears to result mainly from the extensive fragmentation of large stony projectiles in the atmosphere prior to impact.

Many impact craters not associated with meteorites have been recognized on the basis of their shapes, shock-produced features, and absence of evidence for a volcanic origin. Although surface erosion tends to destroy most morphological features within a megayear or less, some very old craters are known (particularly in Canada) that were protected by sediments until recent times, then excavated by selective erosion of the sediments.

Radiometric dating of rocks returned by the Apollo missions to the Moon has revealed that the cratering rate was ~ 100 times greater ~ 4 Gyr ago than it is at present. The Earth was bombarded at that time by the same population of projectiles, so cratering may have played an important role on Earth in excavating and redistributing surficial materials, or in producing cracks through which lava could stream to the surface. A major impact is credited with triggering the magmatic activity responsible for the world's largest deposit of nickel ore near Sudbury, Ontario, Canada.

At 7:17 A.M. on 30 June 1908, an explosion occurred in a remote area of Siberia near the headwaters of the Podkamennaya (Stony) Tunguska River, at about 61°N and 102°E. The air-pressure wave was recorded on seismographs at numerous locations. The region was inhabited mainly by nomadic tribes; because of the remoteness and the unsettled political climate in Russia, no scientific studies of the immediate area were made for nearly two decades. Investigations conducted by Soviet investigators since 1927 have revealed that the explosion flattened trees over a roughly elliptical region of dimensions 40×50 km, and that the exteriors of trees were scorched within a smaller region 15×25 km (Figure I-8). Microbarograph data recorded all around the globe indicate that the energy released during the explosion was $\sim 4 \times 10^{16}$ J, equivalent to that released by exploding 10 Mt of TNT. This amount of energy is ~ 500 times greater than that of an early atomic bomb and is comparable to that of a medium-sized thermonuclear weapon.

The Tunguska explosion produced no crater, and no meteorites have been recovered. A few objects believed to be of extraterrestrial origin have been separated magnetically from local soils or peat, but it is not yet possible to confirm that these are fragments of the projectile. The absence of craters or meteorites fits together with the results of models of the forest devastation to indicate that the explosion occurred at an altitude of about 10 km above the Earth's surface.

Eyewitnesses' observations show that the Tunguska object entered the atmosphere about 660 km south-southeast of the site of the final detonation. The exact velocity cannot be inferred from these observations, but it is estimated to lie in the range of 28 to 47 km · s^{-1}.

How was it possible for the Tunguska object to deposit its entire energy in the atmosphere? Very fanciful suggestions have been made — that the object consisted of antimatter that reacted with ("annihilated") normal matter, or that it was a nuclear-powered alien spacecraft that exploded — but there is no hard evidence favoring such models. It is more likely that the object exploded in the atmosphere because it was friable and underwent total disruption during atmospheric deceleration. A large strong body reaches the Earth's surface at nearly its original velocity, but the same material dispersed as tiny grains can be stopped and its entire kinetic energy converted to thermal energy in the atmosphere. It is commonly accepted that this weak object was a fragment of a comet, and this hypothesis has recently received support from calculations showing that the object's orbit was, like the Taurid meteor streams, consistent with it being a fragment of Encke's comet. Comets are thought to consist of roughly equal parts of silicate grains and water ice, but most ice has evaporated from comets such as Encke that have made repeated passages about the Sun. It seems likely that the Tunguska object consisted mainly of an easily crushed mass of small silicate grains, and it is reasonably probable that it was cometary debris.

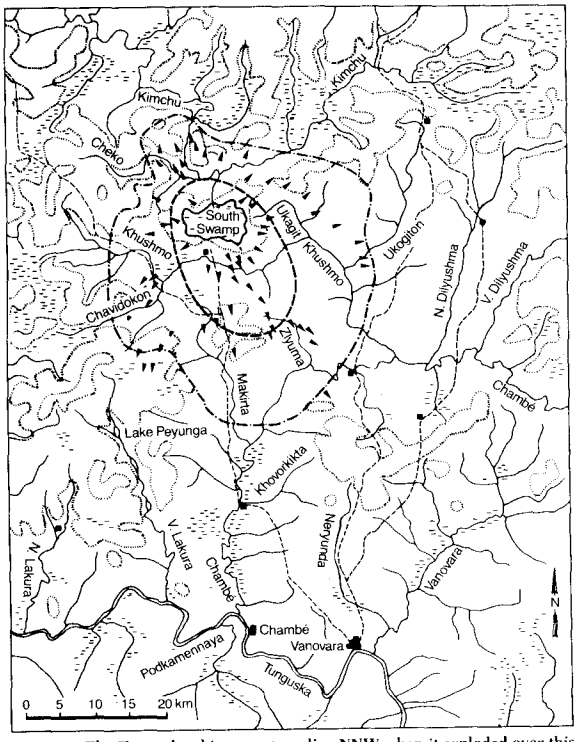

Figure I-8. The Tunguska object was traveling NNW when it exploded over this region labeled South Swamp in a heavily forested area of central Siberia. The radiation from the explosion scorched the trees inside the 15 × 25 km ellipse, and the blast wave flattened trees in the irregularly shaped region having dimensions of about 40 × 50 km. The short arrows show the directions that the trees fell. No meteorites have been recovered, but some particles extracted from the soil may be portions of the meteoroid. The object apparently consisted of weak material that was crushed and disaggregated during atmospheric passage; it probably originated in a comet.

Another remarkable meteoroid that did not reach the Earth's surface was the Rocky Mountains fireball of 10 August 1972, which made a grazing encounter with the Earth's atmosphere before returning to interplanetary space. This object was dazzlingly brilliant, even though seen on a bright early-summer afternoon. It was moving from south to north and was first observed over central Utah and last seen over central Alberta — a distance of ~ 1500 km. It was recorded by the infrared radiometer of a U.S. defense satellite, and these data combined with visual observations from the ground allowed the calculation of an accurate trajectory and orbit. The meteoroid dipped down to within 58 km of the Earth's surface over Montana; sonic booms were heard in this region. Because the trajectory was confined to the thinner part of the atmosphere, its velocity was only reduced 0.8 km · s^{-1} by friction — from 15.0 km · s^{-1} at entry to 14.2 km · s^{-1} at exit from the atmosphere. Estimates of its mass based on the velocity change and its luminosity are roughly congruent at a few thousand tons. Had the object hit the Earth's surface, the energy released would have been ~ 4×10^{12} J, or ~ 1 kt TNT equivalent — comparable to a very small atomic bomb. If the object had been traveling perpendicular to the Earth's surface and had survived passage through the dense part of the atmosphere without fragmentation, it would have excavated a crater with a diameter of 30 to 35 m.

Tektites are curious, small (generally less than 5 cm across), glassy objects that commonly show heat-altered zones characteristic of atmospheric passage. They appear to be melted ejecta produced by major impacts onto silica-rich sedimentary terrains. The absence of silica-rich lunar rocks effectively rules out a suggested lunar origin for these objects. The explosions apparently were so large that the expanding vapor cloud "blew off" the overlying atmosphere and launched the tektites into arching ballistic trajectories that transported them hundreds of kilometers away from the impact site. In a few cases, the parent crater is known. For example, the so-called moldavites recovered in Bohemia, Czechoslovakia, appear to be ejecta from the Ries Crater in southeastern Germany. Other possible associations are listed in Table I-2. The tektites consist almost entirely of terrestrial materials, though in some cases a bit of "meteoritic spice" is present.

The best indicators of meteoritic spice in a terrestrial sample are the siderophile elements (those concentrated in a metallic phase if one is present), especially the noble-metal subset of the siderophiles. Siderophile abundances are very low in crustal rocks because most of the siderophiles originally accreted to the Earth were extracted into the core when it formed, whereas they are present at solar-abundance levels (relative to silicon) in most of the extraterrestrial material accreted to the Earth. One noble metal, iridium (Ir), has abundances in crustal rocks lower than many other noble metals, and its concentration can be determined by the technique of neutron activation at concentrations as low as 1 pg/g (10^{-12} g/g); it

Table I-2
Tektite strewn fields and probable source craters

Tektites	Location	Age (myr)	Crater	
			Name	Location
Australites*	S. Australia	0.71	Not known	——
Indochinites*	Vietnam, Cambodia, Thailand, etc.			
Philippinites*	Philippine Isls.			
Others*†	Indonesia			
Ivory Coast tektites	Ivory Coast	1.15	Lake Bosumtwi	6.5°N 1.4°W
Moldavites	Czechoslovakia	14.0	Nordlinger Ries	48.9°N 10.6°E
Bediasites	Texas, Georgia	34.0	Not known	——
Microtektites‡	Many oceanic locations	Several vintages	——	——

* The groups listed in brackets together comprise the Australasian strewn field. Available evidence indicates that they are cogenetic.
† Rizalites, billitonites, javanites, etc.
‡ Microtektites are associated with the Australasian, Ivory Coast, and North American (bediasite) tektite-producing events and are occasionally found at other levels ("ages") in the sedimentary record.

is therefore the most-commonly used tracer of small amounts of extraterrestrial matter. Much of the iridium in sediments deposited far from land in the central part of the Pacific Ocean is of extraterrestrial origin.

A spectacular discovery of a few years ago is a thin clay layer with exceptionally great iridium concentrations that was deposited all around the world at the boundary between the Cretaceous geologic period (the age of dinosaurs) and the Tertiary geologic period (the age of mammals). The most-plausible explanation of this observation is that a large (5 to 10 km radius) comet or asteroid struck the Earth at that time, and that the many extinctions (including that of the dinosaurs) that occurred then were the result of some dramatic change in the environment caused by this cataclysm. The most-popular suggestion is that the upper stratosphere was filled with very fine dust to the point that no sunlight reached the Earth's surface for several months, and that all members of many species starved or froze during this period of darkness.

Meteorite Recovery

Until the past decade, meteorite recovery depended more on serendipity than planning. Meteorites were either found by people living in the area where an observed fall occurred or, in the absence of fall phenomena, were recognized by farmers, cowboys, prospectors, or rock hounds as being a rock type alien to the area.

Two recent developments that are enhancing meteorite recovery rates are (1) the establishment of photographic networks, and (2) the discovery of concentrations of meteorites in regions where the Antarctic ice sheet is eroding at unusually high rates. The photographic networks consist of arrays of cameras with rotating shutters that are photometrically triggered by bright fireballs. If a fireball is photographed by two stations, an exact trajectory can be established, and the fall site can be fixed to within a few kilometers. To date, the three photographic networks have each recorded one meteorite fall: the Přibram H5 chondrite by the Czech (now joined by the West Germans) All-Sky Network, the Lost City H5 chondrite by the now-defunct U.S. Prairie Network, and the Innisfree L6 chondrite by the Canadian Meteorite Observation and Recovery Project Network.[4] Figure I-9 shows the projection of the orbits of these objects on the ecliptic plane. The yield of new meteorites from these observing networks has been disappointing, but the orbital data are invaluable. The networks also yield precise orbital data for fireballs that fail to produce meteorite finds because the terminal mass is too small or because of unproductive ground searches.

Each orbit shown in Figure I-9 passes into or through the **asteroid belt** (shown stippled), the region between Mars and Jupiter that includes the orbits of all large and most small asteroids. This is an indication that the H-chondrite and L-chondrite parent bodies are (or were) located in the asteroid belt.

A large number of meteorites have been discovered in relatively rock-free areas of the great plains of North America and southwestern Australia. The efficient recovery of meteorites from such areas is partly a result of the educational efforts of H. H. Nininger, G. I. Huss, and other scientists willing to devote their time to field programs.

In 1969, Japanese scientists found nine meteorites of several different classes in an area of a few square kilometers on the Antarctic ice near the Yamato Mountains. During the 1974 and 1975 field seasons, another search party discovered 970 more meteorites in the same general area. The remarkable characteristic of this area is the blue color of the surface that indicates the presence of well-crystallized ice. The value of these cold-stor-

[4] Terminology used to describe meteorites is defined in Chapter II.

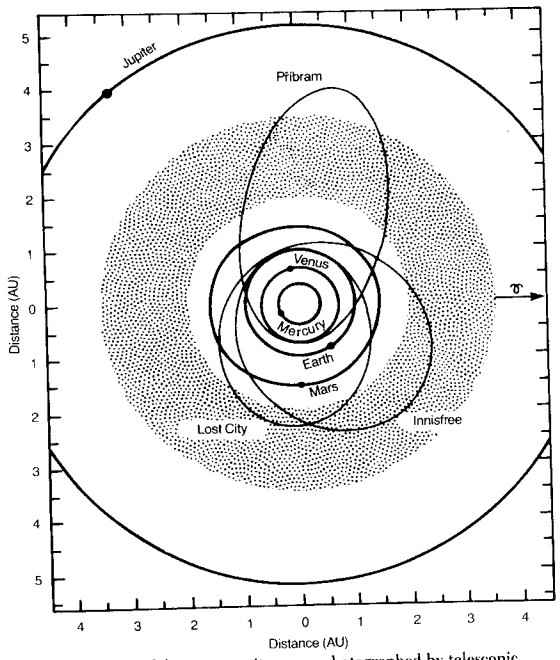

Figure I-9. The falls of three meteorites were photographed by telescopic cameras with rotating shutters. From the photographs, one can determine detailed atmospheric velocities and trajectories and, from this information, accurate orbits. The orbits generally lie in the region between the orbit of Venus and the outer reaches of the asteroid belt (stippled).

age meteorites is now generally recognized, and annual recovery expeditions to Antarctic are being financed by U.S., Japanese, and West German authorities. Terrestrial ages (see Chapter III) as great as ~0.7 Myr have been determined for some of the more weathered meteorites, whereas the fresh, unaltered appearance of others suggests much smaller ages. Because

the temperature below the surface never exceeds 0°C, there is no melting and little mixing between the ice strata produced from the snow accumulated each season.

It is now understood that the blue ice is found in areas where the seaward flow of ice is hampered by mountains (many of them buried). Evaporation and scouring by high winds lead to net evaporation of the ice, exposing meteorites that fell at some other, more-inland location during the past million years. Although most, perhaps all, Antarctic meteorites have been altered by weathering, they are still well suited for many types of research. Their greatest value is in expanding the variety of meteoritic materials in our collections. Each new class of meteorites offers information about solar-system processes and/or locations not previously accessible.

One of the most-striking successes of the Antarctic meteorite-recovery program occurred in the 1981 recovery season with the discovery of a meteorite that almost certainly came from the Moon. It has long been known that a tiny fraction of the material ejected from lunar craters leaves the surface with velocities great enough to allow it to escape the Moon's gravitational field, and that 10 to 30 percent of such materials should eventually reach the Earth's surface. However, until the discovery of the new meteorite (designated Allan Hills A81005), no meteorite having properties closely related to recovered lunar materials was known. Properties indicating that the new stone is a regolith sample from the Moon are its bulk MnO/FeO ratio, oxygen-isotope compositions, cosmic-ray age, content of excess ^{40}Ar, and general mineralogical composition, including a high concentration of anorthite.

Micrometeorites

Small interplanetary dust particles can radiate their frictional energy away fast enough to survive atmospheric deceleration without melting. During the past few decades, attempts to collect these particles in the stratosphere with impactors or filters flown on airplanes, balloons, and rockets have been frustrated by contamination. In 1976, the first successful collections were reported by D. E. Brownlee and colleagues. Individual particles that had impacted onto a collecting plate carried to the stratosphere on a U-2 aircraft were examined in a scanning electron microscope. The researchers found a set of fine-grained particles that show no resemblance to known contaminants. Chondritic concentrations of nonvolatile elements were determined by electron-microscope studies, confirming the extraterrestrial nature of the particles. The particles are more fine-grained and friable than known meteorites, and it is speculated that they are of cometary origin. These particles represent an important new class of solar-system materials that are

available for study in terrestrial laboratories, but their small size (from less than 0.1 μm to ~ 10 μm in diameter) will require the development of new techniques before trace constituents can be determined.

Suggested Reading

Buchwald, V. F. 1975. *Iron Meteorites*. University of California Press. In Volume 1 (of 3) are descriptions of the physics of atmospheric passage (Chapters 3 and 4), craters (Chapter 4) and fall statistics (Chapter 5).

King, E. A. 1976. *Space Geology*. Wiley. Chapter 1 is on meteorites, Chapter 2 on tektites, and Chapters 3 and 4 on craters.

Krinov, E. L. 1966. *Giant Meteorites*. Pergamon. Chapter 3 gives a detailed report on the fall of the Tunguska object.

Mason, B. 1962. *Meteorites*. Wiley. Chapters 1 and 2 give useful historical notes and descriptions of craters and observed falls.

Nininger, H. H. 1952. *Out of the Sky*. Dover. Numerous descriptions of fall phenomena and organized field-recovery programs by an innovative field expert.

Silver, L. T., and P. H. Schultz. 1982. *Geological Implications of Impacts of Large Asteroids and Comets on the Earth*. Special Paper **190**. Geological Society of America. A collection of technical papers presented at a conference stimulated by the evidence for a major impact at the end of the Cretaceous geological period.

Wetherill, G. W. 1974. Solar system sources of meteorites and large meteoroids. *Ann. Rev. Earth Planet Sci.* **2**:303. A technical discussion of evidence relating to meteorite orbits.

Wood, J. A. 1968. *Meteorites and the Origin of Planets*. McGraw-Hill. An introductory-level text. Chapter 1 describes fall phenomena, craters, and observing networks.

CHAPTER II

Composition and Taxonomy

A precise classification system is the key to understanding the biological or geological world; an imprecise system of classification leads to misinterpretations and confusion.

The development of every classificational system follows the same general evolutionary pattern. Properties of the members of the population are surveyed. Some are found to be discontinuous, and a tentative classification is based on these discontinuous properties. Additional surveys reveal other discontinuous properties that can be used to test the initial classification. Every classification scheme continues to evolve as more data become available. Interesting tensions develop between taxonomists who are mainly "lumpers" and those who are mainly "splitters," and between those researchers who are ready (sometimes too ready) to accept changes in a taxonomic system and those who cling to an "established" system long after it has been superceded. These tensions are well exposed at meetings of meteorite researchers.

Taxonomic Principles

The properties of meteorites are not continuous. Detailed studies of the mineralogy, chemical composition, or isotopic composition invariably divide the total population into clusters separated by unpopulated gaps in the distribution. Meteorites that fall together in these clusters in terms of a number of different properties are designated **groups**. For example, there are 13 groups of iron meteorites. Appendix A lists the recognized groups of meteorites. In the case of chondrites, it is sometimes advantageous to divide a group into smaller categories called **types**.

It is not accidental that the members of a group have similar properties. These similar properties result directly from the similar processes that formed the members of the group. Processes of meteorite formation differ from one solar-nebula location to the next and from one parent body to the next. The first step in understanding these processes is to determine which meteorites share a common origin. Then, by careful study of the members of that group, we can produce plausible models to account for their formation.

To simplify the classification, a **group** is required to have five or more members. Clusters consisting of one to four members also exist, but their inclusion in tables such as Appendix A would consume too much space. None of these **ungrouped** meteorites differs radically from the kinds of

meteorites found in the groups. Although they tend to be ignored in summary discussions such as this book, the ungrouped meteorites offer valuable clues regarding early solar-system history, and they are widely studied by meteorite researchers.

Chondrites

The stereotype image of a meteorite is a chunk of iron. In fact, however, iron meteorites account for only a small fraction (about 5 percent) of meteorite falls. The most-common meteorites to fall are the chondrites, stony meteorites with compositions very similar to that of the Sun if the comparison is restricted to nonvolatile elements. The greatest deviations from solar composition are depletions of the most-volatile elements.

In meteorite-research parlance, **abundance** is the atomic ratio of the element of interest relative to a normalizing element, typically silicon. The advantage of using abundances rather than **concentrations** (mass of element divided by mass of sample) is that abundances in diverse samples can be compared even if the total mass of one sample is not known (e.g., in the solar atmosphere) or if the samples differ in their content of some component such as H_2O or metal that may not be relevant to the desired compositional comparison.

In Figure II-1, calcium-normalized solar abundances determined by telescopic measurements of lines in the solar spectrum are compared with those of CI and CM chondrites, the most-volatile-rich classes of chondrites. The agreement between solar and CI abundances is good; the agreement between solar and CM chondrites is good for the nonvolatile elements, but abundances of three well-determined volatiles (Na, K, and Cd in Figure II-1) in CM chondrites are 30 to 50 percent lower than the solar values. The only other chondrite groups having volatile abundances comparable to CM (and lower than CI) levels are the EH and IAB chondrites, but these groups have Si/Ca ratios much higher than the reported solar ratio.

The determination of elements in the Sun is hampered by inadequate knowledge of the formation of spectral lines under the high-temperature (~6000 K) conditions prevailing in the solar photosphere, the visible part of the atmosphere. Because all elements can be determined more precisely in laboratory studies of meteorites, it is common practice to use CI-chondrite abundance data as the best estimate of the composition of the Sun and of the primitive solar nebula from which the planetary portion of the solar system formed. Solar and CI abundances and CI concentration data are tabulated in Appendix D.

The name chondrite was originally based on the observation that such meteorites contain large amounts of small (0.1 to 2 mm) spheroids called

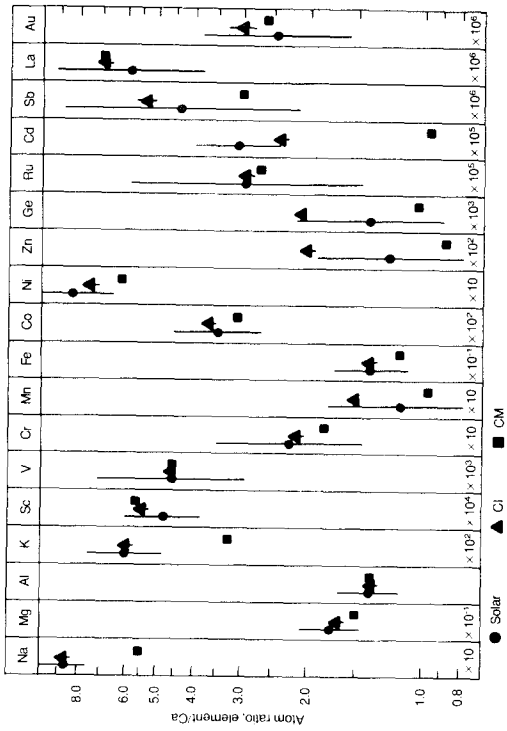

Figure II-1. Comparison of solar and chondritic element/Ca ratios for 18 elements moderately well determined in the solar atmosphere; the vertical bars show 70% confidence limits. Recent CM and CI chondrite abundance data of G. Kallemeyn and J. Wasson agree with the solar values for nonvolatile elements, but only CI abundances for the volatiles sodium, potassium, and cadmium are concordant with solar values. CI chondrites appear to be *the materials most representative of mean*

chondrules (derived from the Greek word for grain; see Chapter VII for a more extensive discussion of chondrules and their origins). The Felix chondrite illustrated in Figure II-2 belongs to a group having a high concentration of choudrules and chondrule fragments. The name *chondrite* is now generally applied to any meteorite having solarlike composition, even though some (such as the volatile-rich CI chondrites just mentioned) are devoid of chondrules.

As discussed in more detail in Chapter VI, it appears that most extrasolar matter was vaporized by the conversion of gravitational to kinetic energy during the formation of the solar system. Gradual cooling of the resulting solar nebula resulted in the sequential condensation of elements in order of decreasing condensation temperatures. Those elements condensing before the **common** elements magnesium, silicon, and iron are designated **refractory** elements.

The abundance of refractory **lithophiles** (elements mainly found in silicate minerals) is nearly constant within each chondrite group but varies considerably among the different groups and, as a result, is a useful parameter for classifying meteorites. Figure II-3 shows silicon-normalized abundances of three refractory lithophiles samarium, scandium, and aluminum plotted against a fourth, calcium. The nine plotted groups of chondrites tend to fall into five clusters on this diagram. Concentrations in a tenth group, the **IAB** chondrites, show considerable scatter, but their mean values fall near those in the L and H groups. Groups that have several properties in common comprise a clan; thus these data indicate five chondrite clans, and the IAB chondrites comprise a sixth. Table II-1 lists group abundances of the refractory elements aluminum and calcium and mean refractory abundances relative to those in CI chondrites.

The degree of oxidation of meteorites is closely related to the distribution of iron among its three common oxidation states, 0, +2, and (more

a CM

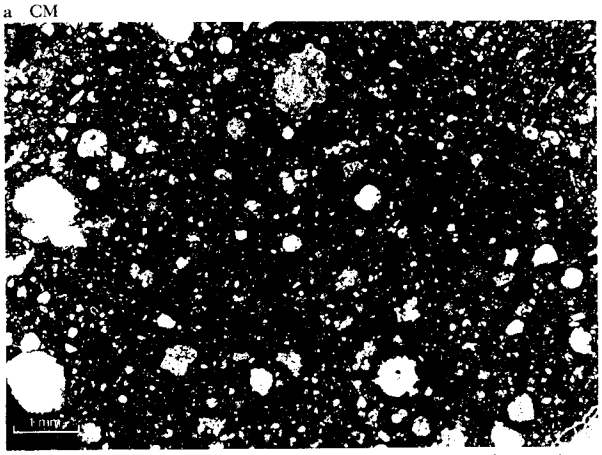

b CO

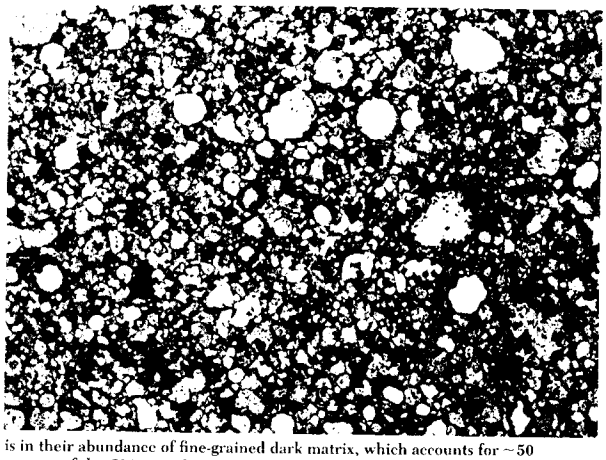

Figure II-2. Thin sections of *(a)* the Murchison CM chondrite and *(b)* the Felix CO chondrite, each photographed in transmitted light. The rounded objects are chondrules, which typically have diameters in the range 0.2 to 0.5 mm in the closely related CM and CO groups. The striking difference between the groups is in their abundance of fine-grained dark matrix, which accounts for ~50 percent of the CM mass, but only 20 to 30 percent of the CO mass. (Photos by W. R. Van Schmus)

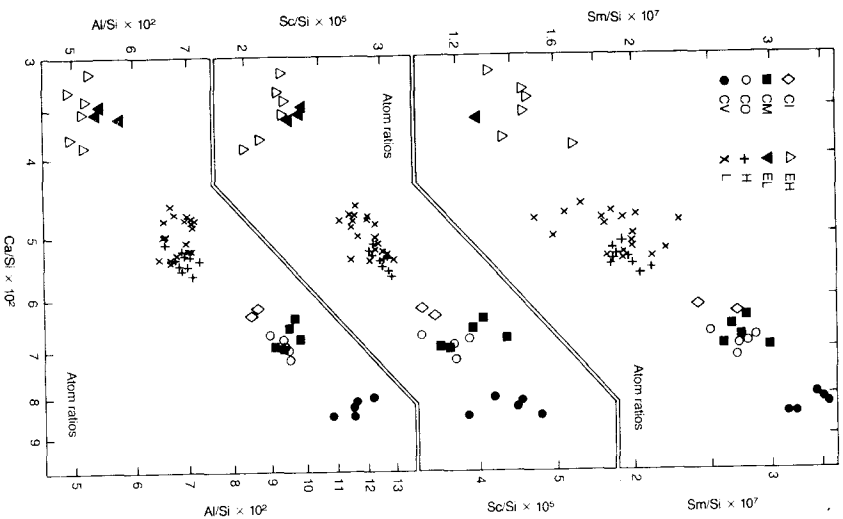

Figure II-3. Refractory-element abundances in the chondrite groups fall into five clusters; individual analyses by G. Kallemeyn are shown. This fractionation of refractories from silicon must have occurred during formation of the chondrites in the solar nebula, because textural evidence shows that no subsequent alteration has occurred. The observed variation makes refractory-element abundance a useful parameter for classifying the chondrites.

Table II-1
Properties of chondrite groups

Clan	Group	Al/Si (atom%)	Ca/Si (atom%)	refr/Si (norm*)	Fe/Si (atom%)	Fe/Si (norm*)	FeO/(FeO + MgO) (mol%)	Mafic-min. comp. (mol%)	Fe met/Si (atom%)	$\delta^{18}O$ (‰)	$\Delta^{17}O$ (‰)	Chondrule size†	Chondrule freq.‡
Refractory-rich	CV	11.6	8.4	1.35	76	0.87	35	§	0.6–19	1	−3	1.0	30
Minichondrule	CO	9.3	6.9	1.10	78	0.90	35	§	2.3–15	0	−4	0.2	70
	CM	9.7	6.8	1.13	80	0.93	43	§	0.1–0.5	7	−3	0.2	2
Volatile-rich	CI	8.6	6.2	1.00	86	1.00	45	§	<0.1	17	+1	—	<1
Ordinary	LL	6.5	4.7	0.76	53	0.62	27	Fa 26–32	2.7–22	4.9	1.3	0.47	80
	L	6.6	4.7	0.77	57	0.66	22	Fa 21–25	17–22	4.6	1.1	0.46	80
	H	6.8	4.9	0.79	80	0.93	17	Fa 17–19	46–52	4.2	0.8	0.33	80
IAB-inclusion	IAB	5–7	4–5	~0.7	~60	~0.70	6	Fs 4–8	~50	5.0	−0.4	—	—
Enstatite	EL	5.4	3.6	0.60	65	0.76	0.05	Fs ~0.05	47–57	5.7	0.0	0.5	—
	EH	5.1	3.6	0.59	97	1.13	0.05	§	68–72	5.7	0.0	0.5	20

* CI-normalized values.
† Median diameter in millimeters.
‡ Frequency as percentage. Metamorphism has destroyed the chondrule record in IAB and EL.
§ Mafic-mineral (olivine, Fa, or low-calcium pyroxene, Fs) compositions given only for equilibrated meteorites.

rarely) + 3. For example, we can write a chemical reaction

$$Fe + \tfrac{1}{2}O_2 = FeO \qquad \text{(II-1)}$$

and for this reaction an equilibrium constant

$$K \simeq \frac{c_{FeO}}{c_{Fe} p_{O_2}^{1/2}} \qquad \text{(II-2)}$$

where c is concentration and p is partial pressure. We will let $p_{O_2}^{1/2}$, the square root of the partial pressure of O_2, be our measure of degree of oxidation. The concentration of Fe in Fe–Ni can generally be set equal to unity, and the concentration of FeO is approximately equal to the FeO/(FeO + MgO) ratio in the ferromagnesian minerals olivine and pyroxene (see mineral formulas in Appendix C). We then obtain the approximate relationship

$$\text{degree of oxidation} \equiv p_{O_2}^{1/2} \propto \frac{FeO}{FeO + MgO} \qquad \text{(II-3)}$$

This relationship is not valid for the CM and CI chondrites in which some iron is present in the +3 state, but it is clear that these groups have higher degrees of oxidation than the highest values observed in the other chondrites having negligible amounts of +3 iron.

The degree of oxidation is also a good classificational parameter; the FeO/(FeO + MgO) ratios listed in Table II-1 range from less than 0.1 to 45 mol%. The values assigned the CM and CI chondrites are their total FeO/(FeO + MgO) ratios but, as noted earlier, their degrees of oxidation are still higher than insertion of this value in Equation II-3 would indicate. The enstatite chondrites are so reduced that some silicon is present as the metal (dissolved in Fe–Ni). Also listed in Table II-1 are the FeO/(FeO + MgO) ratios observed in the mafic minerals olivine and pyroxene; Fa (for fayalite) indicates the ratio in olivine, Fs (for ferrosilite) indicates the ratio in pyroxene.

Another parameter that reflects the degree of oxidation is the fraction of iron present as metal. These values are listed in Table II-1. In Figure II-4, the abundance of reduced iron (defined as that in metal and FeS) is plotted against oxidized-iron abundance. Such a diagram gives a visual representation of both the bulk Fe/Si content (constant values lie along diagonal lines) and the degree of oxidation. Note that the six clans occupy distinct positions, although the separations in the carbonaceous-chondrite region are small.

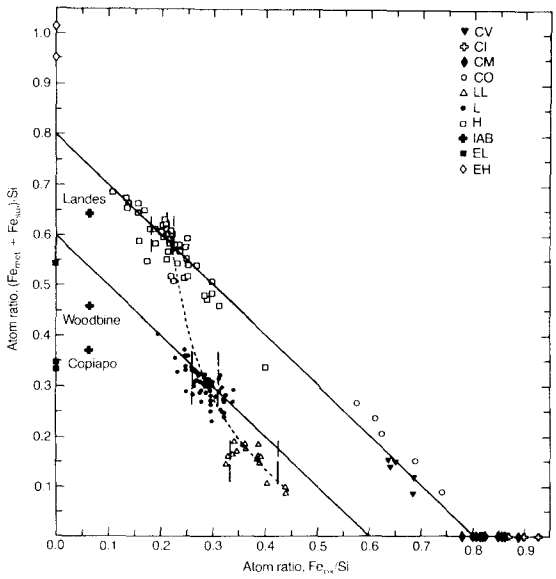

Figure II-4. Chondritic reduced iron (metallic iron and that present as FeS) is plotted against oxidized iron (that present in silicates and, in CM and CI, as Fe_3O_4). Lines having slopes of −1 correspond to constant total Fe/Si ratios; two are shown for reference purposes. A dashed curve depicts a suggested fractionation sequence linking the H (high-iron), L (low-iron) and LL (low-iron, low-metal) ordinary chondrites. The highly reduced enstatite (EH and EL) chondrites plot along the left axis, the highly oxidized CM and CI chondrites along the bottom axis. The fractionations of degree of oxidation and Fe/Si ratio occurred during the formation of these groups in the solar nebula.

Some closely related chondrites differ in their abundances of siderophiles, elements that are concentrated in Fe–Ni if such phases (kamacite and taenite) are present. As discussed in Chapter VIII, these differences appear to result from differing efficiencies in the agglomeration of metal and silicates during planetesimal formation. The abundance of iron shown in Table II-1 is an example of these differences. Note that the groups

comprising the enstatite and ordinary clans are resolved by this parameter.

Variations in the oxygen-isotopic composition are shown in Table II-1 as $\Delta^{17}O$, the difference in the $\delta^{17}O$ value from that expected on the basis of the observed $\delta^{18}O$ value and the 0.52 slope of the terrestrial fractionation line: $\Delta^{17}O = \delta^{17}O - 0.52\delta^{18}O$. See Chapter III for a discussion of oxygen-isotope systematics.

Textural differences are not easily included in a table, but two quantities (the mean abundance and size of chondrules) are included in Table II-1. Other textural and mineralogical features include the grain size, light reflectance, and presence of specified minerals.

As discussed in more detail in Chapters VII, VIII, and IX, the differences between the different chondrite groups almost certainly result from differences in nebular conditions at varying distance from the Sun.

Some chondrites are well equilibrated, with each grain of a given mineral (such as olivine or orthopyroxene) having essentially the same composition, and with the compositions of all minerals in the assemblage being essentially consistent with interequilibration of grains at a "metamorphic" temperature of ~1000 to ~1300 K. In other chondrites, individual minerals show wide ranges in composition, implying formation under very different conditions and little subsequent interequilibration. As discussed further in Chapters VII and VIII, these unequilibrated chondrites best preserve the record of the variety of conditions present in the primitive solar nebula.

It is useful to include in the classification symbol of each chondrite an indication of its degree of equilibration and metamorphic recrystallization. This is done by assigning the chondrites to **petrologic types** ranging from 1 in the least equilibrated to 6 (some workers use 7) in the most-equilibrated chondrites. These numbers are generally appended to the group symbol. Thus Allende is a CV3, Bruderheim an L6, and Abee an EH4 chondrite. Chondrite breccias are classified on the basis of their host fractions. In some ordinary-chondrite breccias, materials ranging from types 3 to 6 coexist.

Other parameters covary with the degree of equilibration and recrystallization. Volatile elements such as hydrogen, carbon, indium, bismuth, and the rare gases generally decrease in abundance with increasing petrologic type. Some components are absent in known type-1 chondrites (all of which are members of the CI group) and present in a systematically varying sequence in the other types. A number of the diagnostic properties are summarized in matrix form in Table II-2, a modified version of that originally proposed by Van Schmus and Wood.

It was earlier held that the least-equilibrated types, 1 and 2, best preserve the record of nebular processes. More recently it has been recognized that these types have been altered by hydrothermal processes which, for example, converted silicate minerals such as olivine to hydrated, clay-like

Table II-2
Criteria for distinguishing different petrologic types of chondrites

	Petrologic type					
	1	2	3	4	5	6
Homogeneity of olivine and pyroxene compositions	——	Mean deviations of pyroxene ≥ 5%, of olivine ≥ 3%		5% > mean pyroxene deviation > 0%	Uniform ferromagnesian minerals	
Structural state of low-Ca pyroxene	——	Predominantly monoclinic		Abundant monoclinic crystals	Orthorhombic	
Degree of development of secondary feldspar	——	Absent		Predominantly as microcrystalline aggregates		Clear, interstitial grains
Igneous glass	——	Clear and isotropic primary glass, variable abundance		Turbid if present	Absent	
Metallic minerals	——	Taenite absent or very minor (Ni < 200 mg/g)	Kamacite and taenite (Ni > 200 mg/g) present			
Mean Ni content of sulfide minerals	——	> 5 mg/g	< 5 mg/g			
Overall texture	No chondrules	Very sharply defined chondrules		Well-defined chondrules	Chondrules readily delineated	Poorly defined chondrules
Texture of matrix	All fine-grained, opaque	Much opaque matrix	Opaque matrix	Transparent microcrystalline matrix	Recrystallized matrix	
Bulk carbon content	30–50 mg/g	8–26 mg/g	2–10 mg/g	< 2 mg/g		
Bulk water content	180–220 mg/g	20–160 mg/g	3–30 mg/g	< 15 mg/g		

Source: R. Van Schmus and J. Wood, *Geochim. Cosmochim. Acta* 31:747 (1967) and more recent results.

minerals. The nebular record is, in fact, best preserved in the least equilibrated type-3 chondrites, as found in groups CO, CV, H, L, LL, and EH.

Differentiated Meteorites

The following scenario appears to be valid for the Earth, and it probably also is valid for the parent planets of some groups of differentiated meteorites. The planet's composition was essentially chondritic, similar to one of the metal-bearing chondrite classes. Complete melting of the interior of such a planet led to the separation of immiscible metal and silicate. The denser metal (the density of solid metal is $\rho = \sim 7.9$ g · cm^{-3}; that of a metallic liquid is somewhat smaller depending on its S content) migrated to the center and formed a core. Further differentiation of the silicates ($\rho = 2.6$ to 3.6 g · cm^{-3}) led to the extrusion of a lighter, fusible silicate melt on the surface, whereas denser and more-refractory silicates remained behind to form a mantle. The differentiated meteorite groups can be fit into such a picture, but it is oversimplified, and a caveat is necessary: each group is stamped by the details of its formation, which often involved multiple melting or mixing events. Properties of differentiated silicate-rich meteorites are listed in Table II-3.

Silicate-rich differentiated meteorites having low metal contents are often designated **achondrites.** The two groups having high metal contents are often called **stony-irons.** The problem with these terms is that they tend to take on unjustified generic significance. For example, the mesosiderite stony-irons and the howardite achondrites are much more closely related than are certain achondrite groups (for example, the howardites and the ureilites). I recommend minimizing the use of the terms achondrite and stony-iron. For mnemonic purposes, it is useful to note that any group given a name that does not include "chondrite" or "iron" is a differentiated silicate-rich meteorite.

On Earth, melting of the mantle generally produces **basalts,** rocks composed of roughly equal amounts of plagioclase and pyroxene. The **eucrites** are a group of basaltic meteorites. Figure II-5 shows a photograph of Ibitira, one of the few eucrites that escaped crushing. The Earth's mantle is composed primarily of ultramafic rocks — rocks having high contents of the mafic ("dark") minerals olivine and (to a lesser extent) pyroxene. The **diogenites** are meteorites having ultramafic compositions. They were previously held to represent the mantle of an asteroid, but alternative proposals involving smaller magmatic systems have recently been proposed. Most eucrites and diogenites have been crushed to form **breccias,** rocks formed from the fragments of preexisting rocks. Because the individual fragments of eucrite and diogenite breccias are from the same rock type, these breccias are designated **monomict.** In some chondrite breccias, the

Table II-3
Properties of differentiated silicate-rich meteorites

Group	Major mafic mineral			Fe–Ni (mg/g)	$\delta^{18}O$ (‰)	$\Delta^{17}O$ (‰)	Breccia type
	Name	Concentration*	FeO/(FeO + MgO) (mol%)				
Eucrites†	Pigeonite	400–800	45–70	<10	3.2–3.8	−0.2	Monomict
Howardites†	Orthopyroxene	400–800	25–40	~10	3.2–3.8	−0.2	Polymict
Diogenites†	Orthopyroxene	~950	25–27	<10	3.2–3.8	−0.2	Monomict
Mesosiderites†	Orthopyroxene	400–800	23–27	300–550	3.2–3.8	−0.2	Polymict
Pallasites†	Olivine	~980	11–14	280–880	3.2–3.8	−0.3	Monomict‡
Aubrites	Low-calcium clinopyroxene	~970	0.01–0.03	~10	5.1–5.5	0.0	Polymict
Ureilites	Olivine	~850	10–25	10–60	7.6–8.0	−1.0	Polymict

* As fraction of silicates.
† Together these five groups comprise the igneous clan.
‡ Pallasitic silicates monomict; metal and silicates probably originally separate in core and mantle, respectively.

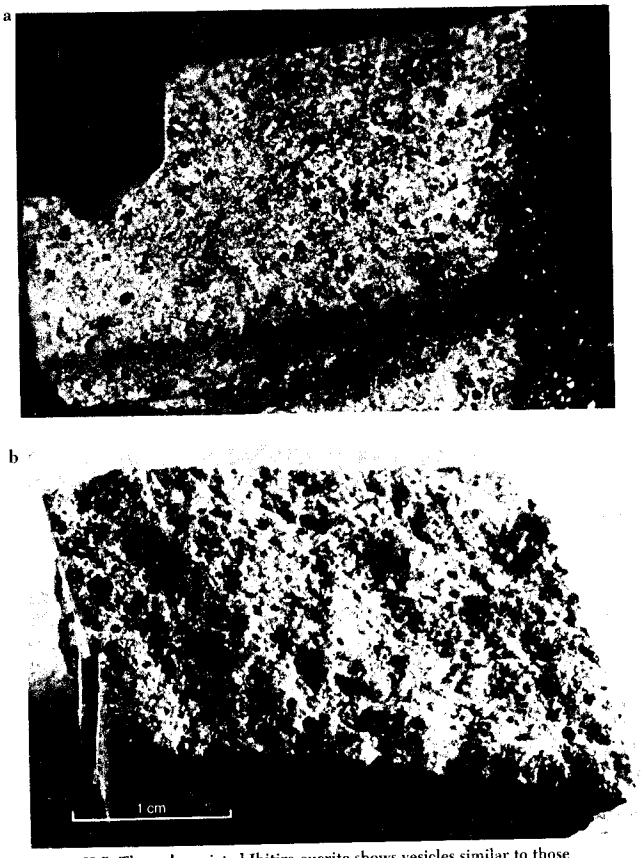

Figure II-5. The unbrecciated Ibitira eucrite shows vesicles similar to those commonly seen in chilled terrestrial lavas. The vesicles resulted from gas formation following extrusion of the basaltic lava into a low-pressure, surficial environment. Before extrusion, the volatile phase was dissolved in the silicate melt. *(a)* The glossy black fusion crust characteristic of eucrites is visible at the top. *(b)* The face is about 2.0 × 2.3 cm. (Photos by F. Wlotzka and P. Deibele)

differences among clasts are only in degree of metamorphic reheating; these breccias are designated **genomict.** Breccias consisting of two or more rock types are designated **polymict.** The **howardites** are polymict breccias containing several rock types but consisting dominantly of rocks similar to the eucrites and the diogenites.

The silicates in the polymict **mesosiderites** are very similar to those in the howardites; the differences are resolvable only by detailed petrological or chemical studies. These curious objects appear to be regolith breccias. The metal may have originated when the surface of an asteroid was impacted by a projectile consisting of a core or core fragment of a fragmented asteroid. This metal seems to have accreted at very low velocity (less than 1 km · s^{-1}), because high-speed impacts lead to low projectile/target ratios in the crater ejecta. Alternative suggestions are that the silicates were the projectile and the metal was exposed on the surface of a large body, or that the metal–silicate ratio in the mesosiderites is not typical of the entire crater ejecta.

The **pallasites** consist of roughly equal portions of metal and the ultramafic mineral olivine. Olivine is probably the dominant mineral in the Earth's mantle, and it is generally accepted that most pallasites originated at the interface between an olivine lower mantle and a metallic core. Three ungrouped pallasites called the Eagle-Station trio have unusual compositions. It has been suggested that they formed from a melt generated by a large impact event on the surface of an undifferentiated parent body.

The oxygen-isotope composition of the eucrites, diogenites, howardites, mesosiderites, and pallasites are very similar (Table II-3). As discussed in more detail in Chapter V, their elemental and phase compositions also appear to be consistent with their joint formation in a single parent body. To emphasize this close relationship, I designated these five groups the **igneous clan.**

The **aubrites** consist almost entirely of the pyroxene enstatite ($MgSiO_3$); its very low iron content indicates an extremely low degree of oxidation, and this is confirmed by the presence of up to 1.2 percent of metallic silicon dissolved in the rare Fe–Ni grains. The oxygen-isotope compositions of aubrites are essentially identical to those in EH and EL chondrites, and the highest metallic-silicon concentrations are identical to those found in the EL chondrites. A close genetic link with the enstatite clan chondrites is thus inferred.

The **ureilites** are curious objects consisting of mixtures of ultramafic silicates with a carbon-rich material that is rich in planetary-type rare gases and thus is apparently primitive in nature (see Chapter III). Diamonds of shock origin are found in the carbon-rich component. Ureilite oxygen-isotope compositions are somewhat similar to those of CM chondrites, well removed from those of other groups of differentiated meteorites.

The ungrouped differentiated silicate-rich meteorites are generally simi-

lar to those just described, but they record distinct differences in formational conditions on other parent bodies. Among these are the shergotty–nakhla–chassigny clan, which shows volatile abundances and isotopic ratios consistent with formation on the surface of Mars. (As discussed in Chapter V, there are some difficulties with this hypothesis of origin.) Information regarding other ungrouped achondrites can be found in more detailed treatises.

Polishing and etching a planar section of an iron meteorite generally reveals a striking structure. Irons consisting entirely of single crystals of **kamacite** (the low-nickel α-iron phase) are called **hexahedrites;** their structures are marked only by the presence of occasional inclusions of FeS or $(Fe,Ni)_3P$ and oriented sets of lines (Neumann lines) of shock origin (Figure I-3). The name *hexahedrite* refers to the fact that these single crystals have cubic (regular hexahedron) crystalline structures. The nickel concentration in hexahedrites is always below 58 mg/g and only rarely below 53 mg/g.

Most irons are **octahedrites** formed by precipitation at 500 to 700°C of kamacite lamellae along four sets of crystalline planes of the high-temperature taenite (γ-iron) phase. The sections through these lamellae exposed on a planar surface are commonly called kamacite bands. This formation, which requires low cooling rates, is discussed in more detail in Chapter IV. The angles between the four sets of planes are identical to those between the faces of a regular octahedron (note that there are only four face orientations in an octahedron because opposite faces are parallel). The thickness to which kamacite lamellae grew depended on the nickel concentration and the parent-body cooling rate: the lower the Ni concentration and/or the lower the cooling rate, the thicker the lamellae. The mean thickness (loosely called the "bandwidth") may range from less than 0.1 mm to several centimeters. To simplify structural descriptions, octahedrites are divided into a bandwidth sequence consisting of finest (less than 0.2 mm), fine (0.2 to 0.5 mm), medium (0.5 to 1.3 mm), coarse (1.3 to 3.3 mm) and coarsest (greater than 3.3 mm) octahedrites. In the older literature, these bandwidth ranges are sometimes treated as classes, but compositional data show that bandwidth measurements alone do not lead to the grouping of genetically related irons.

Figure II-6 shows the structure of the Osseo IAB coarse octahedrite. Such a structure is revealed by polishing a planar surface and etching it with a very dilute solution of nitric acid in ethyl alcohol. The plane of this section is essentially parallel to one of the octahedral planes, which shows up as irregular blotches on the surface. Intersections of lamellae having the other three possible orientations form 60° angles on this surface. The roundish FeS + C inclusions surrounded by $(Fe,Ni)_3P$ are characteristic of group IAB and IIICD irons. They are not found in coarse octahedrite members of other groups (for example, in IIIE irons).

Figure II-7 shows the structure of a large section of the Gibeon IVA fine

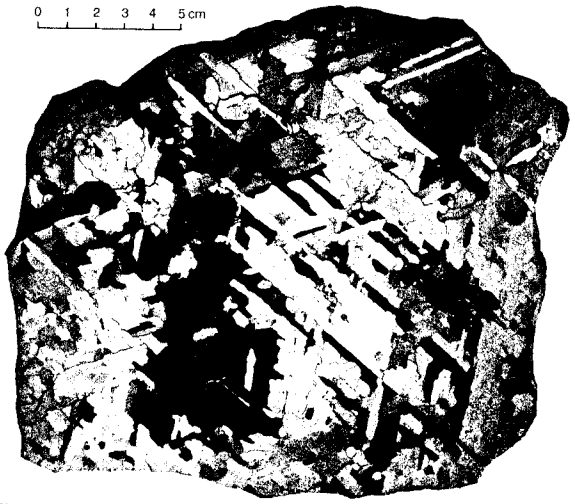

Figure II-6. The Osseo IAB coarse octahedrite consists almost entirely of kamacite bands. This photo made with oblique lighting brings out the contrast in reflectivity even among bands having the same octahedral orientation. Several rounded inclusions consist of medium-gray troilite (FeS) and black graphite (C) surrounded irregularly by light-gray schreibersite ($(Fe,Ni)_3P$). In the upper center, a preterrestrial crack (perhaps of shock origin) has been filled with terrestrial oxidation products. (Smithsonian Institution Photo)

octahedrite. The only inclusions visible in this photo consist of FeS. This section shows discontinuities in the orientation of the **Widmanstätten pattern** (another name for the octahedral structure). The differences reflect the fact that, prior to kamacite precipitation, three distinct taenite crystals occupied these areas; this process is discussed further in Chapter V.

Finely divided mixtures of kamacite and taenite having bulk nickel concentrations greater than ~120 mg/g are called **plessite.** Irons that consist mainly of fine plessite but that also show a few very fine kamacite spindles are designated **plessitic octahedrites.** Figure II-8 shows the Butler plessitic octahedrite, an ungrouped iron. The distinction between finest octahedrites and plessitic octahedrites is that the former have long, continuous

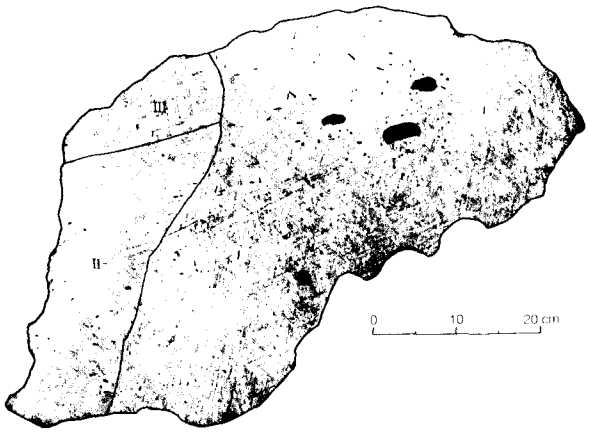

Figure II-7. This large section of the Gibeon IVA fine octahedrite consists of three regions (I, II, and III) having different octahedral orientations of the kamacite lamellae. The dark inclusions are FeS (troilite). Gibeon fell as a gigantic, prehistoric shower in Namibia (South-West Africa). (Photo from R. Schaudy et al., *Icarus* 17:174, 1972)

bands, whereas bands in the latter tend to consist of isolated spindles or intersecting "sparks."

Meteorites whose metallic structure consists entirely of plessite (perhaps with a few rare kamacite prisms) are called **ataxites**, meaning "without structure." Figure II-9 shows an ataxite structure; under careful sample preparation and skilled microscopy, many structural details are visible. The malaprop name dates back to a time when the available microscopes were not adequate to resolve the structure.

Until a decade ago, iron meteorites were classified primarily on the basis of their bandwidths. However, detailed trace-element studies on a large set of iron meteorites revealed that there is only a very rough correlation between structure and compositional groupings. The modern classfication of iron meteorites includes detailed structural study (not just bandwidth measurements) and treats this as information complementary to the chemical composition.

Figure II-8. The ungrouped Butler iron has a plessitic octahedrite structure; kamacite (α-iron) is oriented along the octahedral directions (see text) but forms spindles and sparks rather than long continuous bands. Taenite (γ-iron) is present as darker-gray borders on the lighter-gray kamacite. Between the kamacite "bands" is dark plessite having no visible structure next to the taenite but having tiny, oriented kamacite sparklets in the central regions well away from taenite. The long dimension of the photograph is about 10 mm. (Photo by J. I. Goldstein)

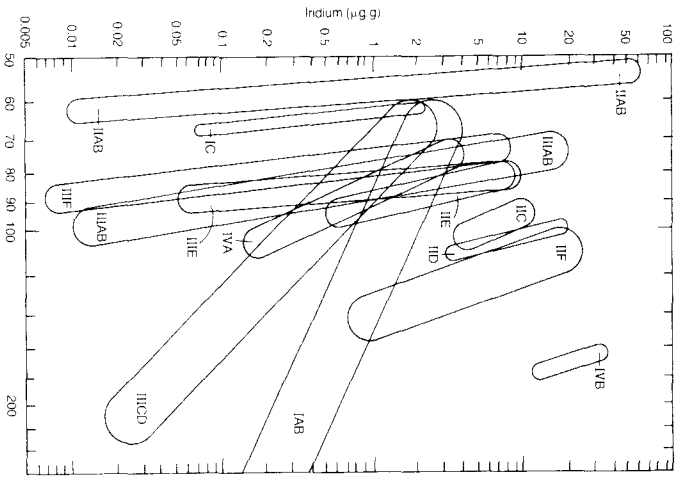

Figure II-11. The concentration of Ir shows large ranges (over factors as large as 6000) in iron-meteorite groups. Because of this large range, iridium concentration is a valuable parameter for determining whether or not two members of a group are fragments from the same fall or are otherwise closely related.

Table II-4
Properties of 13 iron-meteorite and two other metal-rich groups

Group	Freq. (%)	Bandwidth (mm)	Structure*	Ni (mg/g)	Ga (μg/g)	Ge (μg/g)	Ir (μg/g)	Ge–Ni correlation§
IA	17.0	1.0–3	Om–Ogg	64–87	55–100	190–520	0.6–5.5	neg
IB	1.7	0.01–1.0	D–Om	87–250	11–55	25–190	0.3–2.0	neg
IC	2.1	<3	Anom, Og	61–68	49–55	212–247	0.07–2.1	neg
IIA	8.1	>50	H	53–57	57–62	170–185	2–60	pos?
IIB	2.7	5–15	Ogg	57–64	46–59	107–183	0.01–0.9	neg
IIC	1.1	0.06–0.07	Opl	93–115	37–39	88–114	4–11	pos
IID	2.7	0.4–0.8	Of–Om	96–113	70–83	82–98	3.5–18	pos
IIE	2.5	0.7–2	Anom†	75–97	21–28	62–75	1–8	abs
IIF	1.0	0.03–0.21	D–Of	106–140	9–12	99–193	0.8–23	pos
MES	——	ca. 1	Anom	61–101	8.9–16	37–56	2.2–6.2	abs
PAL	——	ca. 0.9	Om	79–129	14–27	29–71	0.01–2	neg?
IIIA	24.8	0.9–1.3	Om	71–93	17–23	32–47	0.15–20	pos
IIIB	7.5	0.6–1.5	Om	84–105	16–21	27–46	0.01–0.15	neg
IIIC	1.4	0.2–3	Off–Ogg	62–130	11–92	8–380	0.07–2.1	neg
IIID	1.0	0.01–0.05	D–Off	160–230	1.5–5.2	1.4–4.0	0.02–0.07	neg
IIIE	1.7	1.3–1.6	Og	82–90	17–19	34–37	0.05–6	abs
IIIF	1.0	0.5–1.5	Om–Og‡	68–85	6.3–7.2	0.7–1.1	0.006–7.9	neg
IVA	8.3	0.25–0.45	Of	74–94	1.6–2.4	0.09–0.14	0.4–4	pos
IVB	2.3	0.006–0.03	D	160–180	0.17–0.27	0.03–0.07	13–38	pos

Note: Brackets combine compositionally distinct portions of single groups.
* Structure abbreviations: H, hexahedrite; Ogg, Og, Om, Of, Off, Opl coarsest, coarse, medium, fine, finest, and plessitic octahedrites; D, ataxite; Anom, anomalous structure that does not fit into the other categories.
† Also Om and Ogg.
‡ Also Ogg and Of.
§Abbreviations: *pos*itive, *neg*ative, *abs*ent.

98 percent of the other irons in the same group. This is very useful when one wishes to determine whether two iron meteorites found within the same area are fragments from the same fall. Table II-4 summarizes the properties of iron meteorites.

Near the beginning of the discussion on iron-meteorite classification I noted that earlier (as recently as two decades ago) the iron meteorites were classified on the basis of bandwidth, but that this did not result in resolved genetically related groups. On the other hand, now that groups have been defined on the basis of compositional and structural evidence, it is possible for an expert to classify a large fraction (perhaps 70 percent) of the iron meteorites on the basis of structural information alone. For example, all single-crystal hexahedrites (Figure I-4) are members of the IIA portion of groups IIAB; all irons with the metal-inclusion texture closely similar to that shown in Figure II-6 are members of group IAB or the closely related minor group IIICD. Fine octahedrites having textures like that of Gibeon (Figure II-7) that are free of inclusions except for minor FeS nodules are almost always members of group IVA.

Compositional studies of the metallic phases of silicate-rich differentiated meteorites also provide valuable classificational information. In this way it has been shown that pallasites divide into one large "main group" and at least two additional compositional clusters. Properties of the metal of mesosiderites and main-group pallasites are also listed in Table II-4.

What is the significance of these groups that have been defined? There is abundant evidence that different groups of the same rock type (different groups of chondrites or irons) were formed in different parent bodies and generally at differing distances from the Sun. In contrast, there exists the possibility that some of the different types of differentiated meteorites (possibly all the members of the igneous clan) formed in the same parent body. These points are discussed in more detail in later chapters.

Suggested Reading

Clayton, R. N., N. Onuma, and T. K. Mayeda. 1976. A classification of meteorites based on oxygen isotopes. *Earth Planet. Sci. Lett.* **30**:10. A technical discussion of the application of oxygen-isotope data to the classification of meteorites.

Dodd, R. T. 1981. *Meteorites: A Petrologic-Chemical Synthesis.* Cambridge University Press. 368 pp. Chondrite classification is discussed in Chapter 2, differentiated-meteorite classification in Chapter 7.

Hutchison, R. 1983. *The Search for Our Beginning.* Oxford University Press. 164 pp. There is much general information about meteorites in this book. Chapter 4 gives a good overview of classification; color plates 3 and 4 show textures of a variety of kinds of meteorites.

Mason, B. 1962. *Meteorites.* Wiley. 274 pp. Chapters 7 and 8 give a good but dated description of the composition and classification of differentiated silicate-rich meteorites.

Scott, E. R. D., and J. T. Wasson. 1975. Classification and properties of iron meteorites. *Rev. Geophys. Space Phys.* **15**:527. The classification of iron meteorites is discussed in detail.

Wasson, J. T. 1974. *Meteorites: Classification and Properties.* Springer. 316 pp. Chapter 2 gives a detailed discussion of meteorite classification.

discussion of the measured properties of the terrestrial and lunar rocks and methods by which these can be inferred to yield the bulk properties of these planets.

Wasson, J. T., and G. W. Wetherill. 1979. Dynamical, chemical and isotopic evidence regarding the formation locations of asteroids and meteorites. In *Asteroids*, ed. T. Gehrels, pp. 926–974. University of Arizona Press. Technical discussion of the dynamical, chemical, and isotopic evidence regarding the formation locations of asteroids and large meteorites.

Wetherill, G. W. 1974. Solar system sources of meteorites and large meteoroids. *Ann. Rev. Earth Planet. Sci.* **2**:303. A technical discussion of the orbital and, less extensively, the compositional evidence regarding the solar-system sources of meteorites and large meteoroids.

Wetherill, G. W. 1979. Apollo objects. *Sci. Amer.* **240**(3):54–65. A relatively nontechnical discussion of the Earth-crossing Apollo asteroids and an evaluation of belt asteroids and comets as sources.

Whipple, F. L. 1978. Comets. In *Cosmic Dust*, ed. J. A. McDonnell, pp. 1–72. Wiley. Moderately technical discussion of observations of comets and inferences regarding cometary properties.

APPENDIX A

Meteorite Classification

Table A-1 lists every meteorite group that contains five or more members and shows the classification into clans that is used in this book.

Table A-1
Classification of meteorites into clans and groups

Clan	Group	Synonyms*	Example	Falls	Finds	Fall frequency† (%)
Chondrites:						
Refractory-rich	CV chon.	C3 carbonaceous	Allende	8	3	1.1
Minichondrule	CO chon.	C3 carbonaceous	Ornans	6	1	0.85
	CM chon.	C2 carbonaceous	Murchison	14	0	2.0
Volatile-rich	CI chon.	C1 carbonaceous	Orgueil	5	0	0.71
Ordinary	LL chon.	Amphoterite chon.	St. Mesmin	51	16	7.2
	L chon.	Hypersthene chon.	Bruderheim	278	192	39.3
	H chon.	Bronzite chon.	Ochansk	229	230	32.3
IAB-inclusion	IAB chon.	——	Copiapo	—‡	—‡	——‡
Enstatite§	EL chon.	Enstatite	Indarch	6	3	0.85
	EH chon.	Enstatite	Khairpur	5	3	0.71
——	Other chon.	——	Kakangari	2	2	0.28
Differentiated meteorites:						
Igneous	Eucrites (EUC)	Basaltic, calcium-rich, or pyroxene–plag. achon.	Juvinas	20	4	2.8
	Howardites (HOW)	Same as EUC	Kapoeta	18	1	2.5
	Diogenites (DIO)	Hypersthene achon.	Johnstown	8	0	1.1
	Mesosiderites (MES)	Stony-irons	Estherville	6	14	0.85
	Pallasites (PAL)	Stony-irons	Krasnojarsk	2	33	0.28
——	Ureilites (URE)	Olivine–pigeonite achon.	Novo Urei	3	3	0.42
Enstatite§	Aubrites (AUB)	Enstatite achon.	Norton County	8	1	1.1
——	Other differentiated silicate-rich meteorites	——	Shergotty	7	6	0.99
——	IAB irons	——	Canyon Diablo	7	83	0.85
——	IC irons	——	Bendego	0	10	0.09
——	IIAB irons	——	Coahuila	5	47	0.49
——	IIC irons	——	Ballinoo	0	7	0.06
——	IID irons	——	Needles	2	11	0.12
——	IIE irons	——	Weekeroo Station	1	11	0.11
——	IIF irons	——	Monahans	0	5	0.05
——	IIIAB irons	——	Henbury	6	151	1.46
——	IIICD irons	——	Tazewell	2	10	0.11
——	IIIE irons	——	Rhine Villa	0	8	0.08
——	IIIF irons	——	Nelson County	0	5	0.05
——	IVA irons	——	Gibeon	2	38	0.38
——	IVB irons	——	Hoba	0	11	0.10
——	Other irons	——	Mbosi	6	62	0.62

Abbreviations: chon. = chondrites; achon. = achondrites; plag. = plagioclase

* Although not used in this book, some of these synonyms are quite common in the current literature. No relevant synonyms exist for the groups of irons.

† Fall frequencies of iron meteorites are calculated by arbitrarily allocating the 32 observed falls confirmed by V. F. Buchwald (*Iron Meteorites*, University of California Press, 1975) to the frequencies of all irons classified by Scott and Wasson (*Rev. Geophys. Space Phys.* 13:530, 1975).

‡ See data for IAB irons.

§ The enstatite-clan chondrites and the aubrites are very closely related.

¶ Clan relationships involving irons are still poorly understood. The only known close relationships are between IIIAB and IIIE irons (possibly also including the pallasites) and between the IIE irons and the H chondrites. Although the structural classification of irons into hexahedrites, octahedrites, and ataxites does not lead to genetically related groups, *most* of the fine octahedrites belong to group IVA, *most* of the medium octahedrites to group IIIAB, *most* of the coarse octahedrites to subgroup IA, and *all* of the large-crystal (at least 5 cm) hexahedrites to subgroup IIA.

APPENDIX B

Units and Constants

Table B-1 lists the units used in this book; it also includes the value of the gravitational constant G.

The International System of Units (Système International d'Unités, or SI) was established in 1960 by international agreement. Seven SI base units are defined in terms of actual physical phenomena: the meter (metre), the kilogram, the second, the ampere, the kelvin, the mole, and the candela (a unit of luminous intensity). All other SI units are derived units that are defined terms of the base units. Table B-2 lists the prefixes that can be used with any SI unit to indicate multiples or submultiples of that unit.

Some non-SI units are still used commonly in astronomical literature; the SI equivalents of such units used in this book are given in Table B-1.

Table B-1
Units and constants

Unit or constant	Abbreviation	Quantity	Equivalent to
Atmosphere	atm	Pressure	10^5 Pa = 10^5 N · m^{-2}
Astronomical unit	AU	Length	1.50×10^{13} cm
Electron volt	eV	Energy	1.60×10^{-19} J
Gram	g	Mass	10^{-3} kg
Gravitational constant	G	——	6.67×10^{-8} cm^3 · g^{-1} · s^{-2}
Joule	J	Energy	1 m^2 · kg · s^{-2} = 1 N · m
Kelvin	K	Thermodynamic temperature	
Mass of Earth	$M_\oplus$	Mass	5.98×10^{27} g
Mass of Sun	$M_\odot$	Mass	1.00×10^{33} g
Meter (metre)	m	Length	100 cm
Mole	mol	Amount of substance	
Newton	N	Force	1 m · kg · s^{-2}
Parsec	pc	Length	3.09×10^{18} cm
Tonne (metric ton)	t	Mass	10^6 g
Second	s	Time	——
Year	yr	Time	3.16×10^7 s

Table B-2
SI prefixes

Prefix	Abbreviation	Multiplier
pico-	p	10^{-12}
nano-	n	10^{-9}
micro-	μ	10^{-6}
milli-	m	10^{-3}
centi-*	c	10^{-2}
kilo-	k	10^3
mega-	M	10^6
giga-	G	10^9
tera-	T	10^{12}

* Centi-, while not an SI prefix, is used in the text and is listed for convenience.

APPENDIX C

Common Meteoritic Minerals

Table C-1 lists the minerals most commonly found in meteorites and gives their chemical formulas.

Table C-1
The most-common meteoritic minerals

Mineral	Formula	Remarks
Albite	$NaAlSi_3O_8$	Component of plagioclase
Anorthite	$CaAl_2Si_2O_8$	Component of plagioclase
High-calcium clinopyroxene	$Ca_xAl_{2y}(Mg,Fe)_{1-x-y}Si_{1-y}O_3$	$x \cong 0.45$; $y \leq 0.05$
Low-calcium clinopyroxene	$Ca_x(Mg,Fe)_{1-x}SiO_3$	$x \leq 0.05$ (see pigeonite)
Cohenite	$(Fe_xNi_{1-x})_3C$	$x \cong 0.9$
Diopside	$Ca_{0.5}Mg_{0.5}SiO_3$	A form of high-calcium clinopyroxene
Fayalite	Fe_2SiO_4	Component of olivine
Ferrosilite	$FeSiO_3$	Component of pyroxene
Forsterite	Mg_2SiO_4	Component of olivine
Kamacite	Fe_x–Ni_{1-x}	$0.96 \leq x \leq 0.93$
Oldhamite	CaS	—
Olivine	$(Mg,Fe)_2SiO_4$	See fayalite, forsterite
Orthopyroxene	$Ca_x(Mg,Fe)_{1-x}SiO_3$	$x \leq 0.05$
Pigeonite	$Ca_x(Mg,Fe)_{1-x}SiO_3$	$x \cong 0.1$; a clino-pyroxene
Plagioclase	$(NaSi)_x(CaAl)_{1-x}AlSi_2O_6$	$0.1 < x < 0.9$
Schreibersite	$(Fe_xNi_{1-x})_3P$	$x \cong 0.7$
Taenite	Fe_x–Ni_{1-x}	$0.5 \leq x \leq 0.8$
Troilite	FeS	—

APPENDIX D

Solar-Atmosphere and CI-Chondrite Atomic Abundances

The CI carbonaceous chondrites are the chondrites having the highest contents of volatiles. As shown in Figure II-1, the most-accurately determined solar abundances[1] of volatile elements show good agreement with volatile abundances in CI chondrites but are significantly higher than those in CM chondrites (the group having the second-highest abundances of volatiles).

The CI chondrites can be studied in the laboratory, and their elemental concentrations (with few exceptions) have been determined with good accuracy. Silicon-normalized CI abundances are accurate to ±10 percent. Solar abundances are determined mainly by telescopic spectroscopic studies of lines produced by absorption or emission at various depths (and pressures and temperatures) in the hot solar atmosphere, and these values are rarely precise to better than ±20 percent. For this reason, data on the CI chondrites are believed to offer the best estimates of mean solar or solar-nebula compositions except for the incompletely accreted, most-volatile elements: hydrogen, carbon, nitrogen, oxygen, and the rare-gas elements.

Table D-1 lists solar-abundance data from J. E. Ross and L. H. Aller and CI-chondrite data compiled especially for this text. The CI-chondrite data are based on a survey of the literature through June 1983. Because there is considerable variation in the quality of the data, a selection must be made. The references actually used are cited in Table D-1.

Another recent compilation by E. Anders and M. Ebihara[2] gives a more complete listing of relevant CI data sources and criteria for choosing values when data are lacking or show excessive scatter. Their selected CI concentrations for beryllium, boron, rhodium, tantalum, mercury, and the 14 rare-earth elements lanthanum through lutetium are used in Table D-1. My CI concentrations for the remaining 59 elements agree with those of Anders and Ebihara to within +5 percent with the exception of nine elements. Six of these (carbon, sulfur, yttrium, niobium, antimony, and osmium) agree to within ±10 percent; for the remaining three, the ratios of their value to mine are 0.88 for nitrogen, 1.20 for phosphorus, and 0.87 for iodine.

[1] An abundance is the atomic ratio of the element of interest to a normalizing element, commonly silicon.

[2] E. Anders and M. Ebihara. 1982. Solar system abundances of the elements. *Geochim. Cosmochim. Acta* 46:2363–2380.

One good method to test the quality of abundance data is to plot the logarithm of nuclide[3] abundance versus mass number and examine whether the tabulated abundances lead to smooth variations. Figure D-1 shows such a diagram for the mass-number range of 21 through 209. Below mass number 21, most elemental abundances have high uncertainties; between mass numbers 209 and 232, all nuclides have half-lives that are short compared to the 4.5 Gyr age of the solar system and, because of this large hiatus, points for the long-lived ($T_{1/2} > 1$ Gyr) ^{232}Th, ^{235}U, and ^{238}U are not plotted.

Separate curves are described by the abundances of even-mass-number and old-mass-number nuclides (Figure D-1). The even-mass-number curve is generally higher by ~ 0.3 log units, but in a few cases the curves become superposed. The simplest explanation of this discrepancy is the following. At mass numbers of 36 or more, there are two or three stable nuclides for each even mass number whereas, with rare exceptions, there is only one stable nuclide for each odd mass number.

A more-correct explanation is that proton or neutron pairs are especially stable. Said another way, an "even" proton has about 2 MeV more binding energy[4] than does an "odd" proton, and the extra binding energy is similar for "even" neutrons. The stable even-mass-number nuclides thus have ~ 2 MeV more binding energy than do neighboring stable odd-mass-number nuclides, and this higher stability is an additional factor accounting for the higher integrated abundances of even-mass-number nuclides. An interesting byproduct of the difference in the binding energies of odd and even protons or neutrons is that odd-atomic-number, odd-neutron-number (odd–odd) nuclides are unstable with respect to beta decay to even–even nuclides; the few odd–odd nuclides above mass number 14 that exist in nature are radioactive.

Most heavy nuclides (mass number at least 60) were formed by neutron capture, and the abundance of a nuclide produced by this process is inversely proportional to its cross-section (a measure of the probability of neutron capture). The extra stability of the even–even nuclides results in their average cross-sections being somewhat lower than those of neighboring odd-mass-number nuclides. In some regions the even-mass-number curve is zigzag, particularly at mass numbers 56 or less, where the capture of α particles (^{4}He nuclei) is an important mode of nucleosynthesis. The odd-mass-number curve is remarkably smooth; its peaks are round rather than jagged. In those cases where an element has two stable nuclides, the local slope is determined by their relative isotopic abundances, and these elements can sometimes be used to confirm general trends in particular mass-number regions. An example is the existence of the valley at mass number 135.

The various peaks appearing in Figure D-1 reflect high efficiencies of certain nucleosynthesis processes in these mass-number regions. For example, the peak near mass number 56 is attributed to an approach to "nuclear equilibrium" in the centers of very hot stars; these abundant nuclides have minimum values of mass/mass-number ratios, or maxima in binding energy per mass number. The peak near mass number 194 is attributed to the effect of a closed shell at neutron number 128 during neutron capture on a rapid time scale.

The scope of this book does not permit giving more details on this fascinating subject. An excellent treatise at an upperclass textbook level is that by J. Audouze and S. Vauclair.[5] A more-technical recent book is the volume of essays by experts in the field edited by C. A. Barnes et al.[6]

[3] As defined in Chapter III, a **nuclide** is an atomic or nuclear species characterized by any two of the three quantities atomic number, neutron number, and mass number. Thus $^{12}_{6}$C is a nuclide having 6 protons and 6 neutrons, which combine to give a mass number of 12.

[4] **Binding energy** is the difference in energy or mass between the free and the bound proton or neutron. For example, when a neutron is added by the reaction

$$^{A-1}_{Z}X + {}^{1}_{0}n = {}^{A}_{Z}X + BE$$

then BE is the binding energy of that neutron.

[5] Audouze, J., and S. Vauclair 1980. *An Introduction to Nuclear Astrophysics*. Reidel.

[6] Barnes, C. A., D. D. Clayton, and D. N. Schramm, eds. 1982. *Essays in Nuclear Astrophysics*. Cambridge University Press.

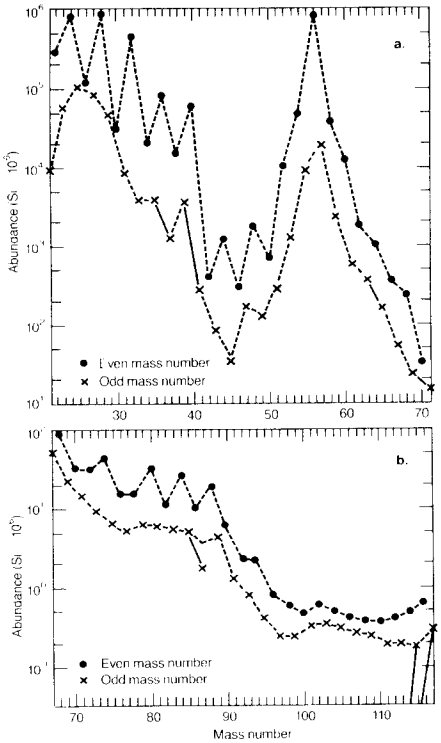

Figure D-1. Solar abundances of elements plotted against the mass number (the number of protons plus neutrons in the nuclide). The even-mass-number abundances tend to be several times higher than those of odd-mass-number nuclides. In some mass ranges, the even-mass-number curve is zigzag whereas, with rare exceptions, the odd-mass-number curve is smooth. For this reason the odd-mass-number curve can be used to test data quality or to search for fractionations occurring during the formation of the CI chondrites. If an element has more than one stable odd-mass-number nuclide, these are connected by a solid line; such cases are valuable because they unambiguously establish the slope of the curve in these regions. In those few cases where two stable odd-mass-number nuclides have the same mass, both points are plotted, but the curve is drawn through the total abundance.

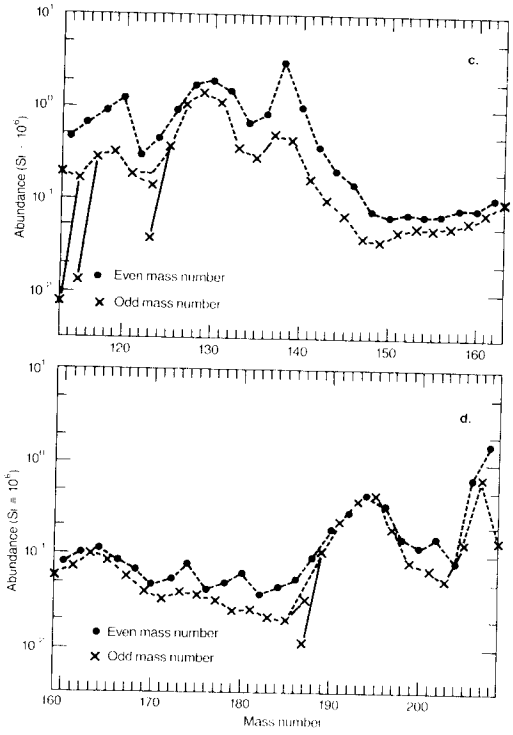

Table D-1
A new compilation of elemental concentration and abundance data for CI chondrites, and a comparison with abundances in the solar atmosphere

Atomic number	Element	Symbol	Solar abundance*	CI chondrites			
				Abundance	Concentration		References
1	Hydrogen	H	2.2×10^{10}	—†	20	mg/g	Wi69
2	Helium	He	2.3×10^{9}	—†	18	ng/g	Ma70
3	Lithium	Li	2.2×10^{-1}	6.05×10^{1}	1.57	μg/g	Ni74
4	Beryllium	Be	3.2×10^{-1}	8.01×10^{-1}	27	ng/g	An82
5	Boron	B	9.1×10^{0}	2.47×10^{1}	1.0	μg/g	An82, Cu80
6	Carbon	C	1.0×10^{7}	—†	32	mg/g	Wi69
7	Nitrogen	N	2.2×10^{6}	—†	1.5	mg/g	In74, Ke83, Ro82
8	Oxygen	O	1.9×10^{7}	—†	460	mg/g	Wi69
9	Fluorine	F	8.1×10^{2}	9.01×10^{2}	64	μg/g	Dr79, Go74
10	Neon	Ne	2.6×10^{6}	—†	300	pg/g	Ma70
11	Sodium	Na	4.7×10^{4}	5.59×10^{4}	4.8	mg/g	Ka81
12	Magnesium	Mg	9.6×10^{5}	1.07×10^{6}	97	mg/g	Ah69, Ka81, Wi69
13	Aluminum	Al	7.4×10^{4}	8.53×10^{4}	8.6	mg/g	Dr80, Ka81, Lo69, Wa74
14	Silicon	Si	$=1.0 \times 10^{6}$	$=1.00 \times 10^{6}$	105	mg/g	Ah69, Kn81, Wi69
15	Phosphorus	P	6.9×10^{3}	8.81×10^{3}	1.02	mg/g	Ah69
16	Sulfur	S	3.9×10^{5}	4.9×10^{5}	59	mg/g	Wi69
17	Chlorine	Cl	7.1×10^{3}	5.13×10^{3}	680	μg/g	Dr79
18	Argon	Ar	8.5×10^{4}	—†	1.3	ng/g	Ma70
19	Potassium	K	3.2×10^{3}	3.83×10^{3}	560	μg/g	Ah69, Ka81, Mi79, Ni74
20	Calcium	Ca	5.0×10^{4}	6.14×10^{4}	9.2	mg/g	Ah69, Ka81
21	Scandium	Sc	2.8×10^{1}	3.45×10^{1}	5.6	μg/g	Ka81, Sc64
22	Titanium	Ti	2.6×10^{3}	2.35×10^{3}	420	μg/g	Ah69, Dr80, Wa74, Wi69
23	Vanadium	V	3.0×10^{2}	2.94×10^{2}	56	μg/g	Ka81
24	Chromium	Cr	1.3×10^{4}	1.36×10^{4}	2.65	mg/g	Ka81
25	Manganese	Mn	6.0×10^{3}	9.25×10^{3}	1.90	mg/g	Ah69, Ka81, Pa78
26	Iron	Fe	8.5×10^{5}	8.72×10^{5}	182	mg/g	Ah69, Ka81
27	Cobalt	Co	2.0×10^{3}	2.31×10^{3}	508	μg/g	Ka81, Sc72
28	Nickel	Ni	4.3×10^{4}	4.88×10^{4}	10.7	mg/g	Ch76, Eb82, Ka81
29	Copper	Cu	2.6×10^{2}	5.09×10^{2}	121	μg/g	Kn81, Sc72, Wa74
30	Zinc	Zn	5.7×10^{2}	1.28×10^{3}	312	μg/g	Ch76, Eb82, Ia78, Ka81, Kr73
31	Gallium	Ga	1.4×10^{1}	3.76×10^{1}	9.8	μg/g	Ch76, Fo67a, Kn81
32	Germanium	Ge	7.1×10^{1}	1.22×10^{2}	33	μg/g	Ch76, Eb82, Fo67a, Ka81, Kr73, Ta78
33	Arsenic	As	5.9×10^{0}	6.57×10^{0}	1.84	μg/g	Ca72, Fo67b, Ka81
34	Selenium	Se	1.8×10^{1}	6.64×10^{1}	19.6	μg/g	Eb82, Ka81, Kr73, Ta78
35	Bromine	Br	NBV	1.21×10^{1}	3.6	μg/g	Go67, Ka81, Ta78
36	Krypton	Kr	4.7×10^{1}	—†	33	pg/g	Ma70
37	Rubidium	Rb	5.9×10^{0}	6.95×10^{0}	2.22	μg/g	Mi79
38	Strontium	Sr	1.8×10^{1}	2.41×10^{1}	7.9	μg/g	Ka70, Kn81, Mi79
39	Yttrium	Y	4.0×10^{0}	4.33×10^{0}	1.44	μg/g	Sc64
40	Zirconium	Zr	1.0×10^{1}	1.11×10^{1}	3.8	μg/g	Ga76, Kn81, Sh79, Wa74
41	Niobium	Nb	1.8×10^{0}	7.77×10^{-1}	270	ng/g	Gr72
42	Molybdenum	Mo	1.9×10^{0}	2.57×10^{0}	920	ng/g	Pa81
43	Technetium‡	Tc	—	—	—	—	—
44	Ruthenium	Ru	1.5×10^{0}	1.88×10^{0}	710	ng/g	Cr67, Ka81
45	Rhodium	Rh	5.6×10^{-1}	3.48×10^{-1}	134	ng/g	An82
46	Palladium	Pd	7.1×10^{-1}	1.41×10^{0}	560	ng/g	Eb82, Fo67b, Ka81
47	Silver	Ag	1.6×10^{-1}	5.16×10^{-1}	208	ng/g	Eb82, Kr73, Ta78
48	Cadmium	Cd	1.6×10^{0}	1.55×10^{0}	650	ng/g	Ch76, Eb82, Ka81, Kr73, Ta78
49	Indium	In	1.0×10^{0}	1.86×10^{-1}	80	ng/g	Ch76, Eb82, Fo67a, Ka81, Ta78

Table D-1 *(continued)*

Atomic number	Element	Symbol	Solar abundance*	CI chondrites			References
				Abundance	Concentration		
50	Tin	Sn	2.0×10^{0}	3.88×10^{0}	1.72	μg/g	Eb82, Ha69, Kn81
51	Antimony	Sb	2.2×10^{-1}	3.36×10^{-1}	153	ng/g	Ca72, Eb82, Fo67b, Ka81, Kn81, Kr73
52	Tellurium	Te	NRV	5.03×10^{0}	2.4	μg/g	Eb82, Sm77
53	Iodine	I	NRV	1.05×10^{0}	500	ng/g	Dr79, Go67, Re66
54	Xenon	Xe	5.4×10^{0}	—†	32	pg/g	Ma70
55	Cesium	Cs	$<1.8 \times 10^{0}$	3.68×10^{-1}	183	ng/g	Eb82, Ke73, Mi79, Pa78, Sm64, Ta78
56	Barium	Ba	2.8×10^{0}	4.48×10^{0}	2.3	μg/g	Kn81, Na74, Re67
57	Lanthanum	La	3.0×10^{-1}	4.55×10^{-1}	236	ng/g	An82, Ev78
58	Cerium	Ce	7.9×10^{-1}	1.18×10^{0}	616	ng/g	An82, Ev78
59	Praseodymium	Pr	1.2×10^{-1}	1.76×10^{-1}	92.9	ng/g	An82, Ev78
60	Neodymium	Nd	3.8×10^{-1}	8.48×10^{-1}	457	ng/g	An82, Ev78
61	Promethium‡	Pm	—	—	—		—
62	Samarium	Sm	1.4×10^{-1}	2.65×10^{-1}	149	ng/g	An82, Ev78
63	Europium	Eu	1.1×10^{-1}	9.86×10^{-2}	56.0	ng/g	An82, Ev78
64	Gadolinium	Gd	3.0×10^{-1}	3.35×10^{-1}	197	ng/g	An82, Ev78
65	Terbium	Tb	NRV	5.98×10^{-2}	35.5	ng/g	An82, Ev78
66	Dysprosium	Dy	2.6×10^{-1}	4.03×10^{-1}	245	ng/g	An82, Ev78
67	Holmium	Ho	NRV	8.87×10^{-2}	54.7	ng/g	An82, Ev78
68	Erbium	Er	1.3×10^{-1}	2.56×10^{-1}	160	ng/g	An82, Ev78
69	Thulium	Tm	4.1×10^{-2}	3.91×10^{-2}	24.7	ng/g	An82, Ev78
70	Ytterbium	Yb	1.8×10^{-1}	2.46×10^{-1}	159	ng/g	An82, Ev78
71	Lutetium	Lu	1.3×10^{-1}	3.75×10^{-2}	24.5	ng/g	An82, Ev78
72	Hafnium	Hf	1.7×10^{-1}	1.80×10^{-1}	120	ng/g	Ga76, Kn81, Sh79, Wa74
73	Tantalum	Ta	NRV	2.51×10^{-2}	16	ng/g	Dr80
74	Tungsten	W	1.1×10^{0}	1.46×10^{-1}	100	ng/g	Wa74
75	Rhenium	Re	3.1×10^{-1}	5.12×10^{-2}	37	ng/g	Eb82, Fo67b, Kr73, Mo67, Ta78
76	Osmium	Os	1.1×10^{0}	6.89×10^{-1}	490	ng/g	Eb82, Ka81, Ta78
77	Iridium	Ir	6.5×10^{-1}	6.40×10^{-1}	460	ng/g	Ch76, Eb82, Ka81, Kr73, Pa81, Ta78
78	Platinum	Pt	1.3×10^{0}	1.36×10^{0}	990	ng/g	Cr67, Eb82, Eh72, Kn81, Wa74
79	Gold	Au	1.3×10^{-1}	1.96×10^{-1}	144	ng/g	Ka81, Kr73, Ta78, Wa74
80	Mercury	Hg	$<2.8 \times 10^{0}$	5.20×10^{-1}	390	ng/g	An82, Re67
81	Thallium	Tl	1.8×10^{-1}	1.86×10^{-1}	142	ng/g	Eb82, Kr73, Re50, Ta78
82	Lead	Pb	1.9×10^{0}	3.10×10^{0}	2.4	μg/g	Ta76
83	Bismuth	Bi	$<1.8 \times 10^{0}$	1.41×10^{-1}	110	ng/g	Kr73, La70, Ta78
84–89	Unstable elements		—	—	—		—
90	Thorium	Th	3.5×10^{-2}	4.34×10^{-2}	29	ng/g	Mo68, Ta76
91	Protactinium‡	Pa	—	—	—		—
92	Uranium	U	$<8.9 \times 10^{-2}$	9.22×10^{0}	8.2	ng/g	Kr73, Ta76, Ta78

* Solar-abundance data from J. E. Ross and L. H. Aller, *Science* **191**:1223 (1976), as updated by L. H. Aller, to be published in *Spectroscopy and Astrophysical Plasmas*, eds. A. Dalgarno and D. Layzer, University of Cambridge, 1985. NRV = No reliable value; CI-chondrite abundances provide the best-available estimates of solar abundances for these elements.

† Volatile element for which no abundance was calculated. These elements are severely depleted in CI chondrites.

‡ Unstable element.

References:

Ah69 Ahrens, L., et al. 1969. *Earth Planet. Sci. Lett.* **6**:285.

An82 Anders, E., and M. Ebihara. 1982. *Geochim. Cosmochim. Acta* **46**:2363.

Ca72 Case, D., et al. 1972. *Geochim. Cosmochim. Acta* **36**:19–33.

Ch76 Chou, C.-L., et al. 1976. *Geochim. Cosmochim. Acta* **40**:85–94.

Cr67 Crocket, J. H., et al. 1967. *Geochim. Cosmochim. Acta* **31**:1615–1623.

Cu80 Curtis, D., et al. 1980. *Geochim. Cosmochim. Acta* **44**:1945–1953.

Dr79 Dreibus, G., et al. 1979. *Origin and Distribution of the Elements*, pp. 33–38. Pergamon.

Dr80 Dreibus, G., and H. Wänke. 1980. *A. Naturforsch.* **35a**:204–216.

Table D-1 *(continued)*

Eb82 Ebihara, M., et al. 1982. *Geochim. Cosmochim. Acta* **46**:1849–1862.
Eh72 Ehmann, W. D., and D. E. Gillum. 1972. *Chem. Geol.* **9**:1–11.
Ev78 Evensen, N. M., et al. 1978. *Geochim. Cosmochim. Acta* **42**:1199–1212.
Fo67a Fouché, K. F., and A. A. Smales. 1967. *Chem. Geol.* **2**:5–33.
Fo67b Fouché, K. F., and A. A. Smales. 1967. *Chem. Geol.* **2**:105–134.
Ga76 Ganapathy, R., et al. 1976. *Earth Planet. Sci. Lett.* **29**:302–308.
Go67 Goles, G. G., et al. 1967. *Geochim. Cosmochim. Acta* **31**:1771–1787.
Go74 Goldberg, R. H., et al. 1974. *Meteoritics* **9**:347–348.
Gr72 Graham, A. L., and B. Mason. 1972. *Geochim. Cosmochim. Acta* **36**:917–922.
Ha69 Hamaguchi, H., et al. 1969. *Geochim. Cosmochim. Acta* **33**:507–518.
In75 Injerd, W. G., and I. R. Kaplan. 1975. *Meteoritics* **9**:352–353.
Ka70 Kaushal, S. K., and G. W. Wetherill. 1970. *J. Geophys. Res.* **75**:463–468.
Ka81 Kallemeyn, G. W., and J. T. Wasson. 1981. *Geochim. Cosmochim. Acta* **45**:1217–1230.
Ke83 Kerridge, J. R. 1983. In preparation.
Kn81 Knab, H.-J. 1981. *Geochim. Cosmochim. Acta* **45**:1563–1572.
Kr73 Krähenbühl, U., et al. 1973. *Geochim. Cosmochim. Acta* **37**:1353–1370.
La70 Lal, J. C., et al. 1970. *Geochim. Cosmochim. Acta* **34**:89–103.
Lo69 Loveland, W., et al. 1969. *Geochim. Cosmochim. Acta* **33**:375–385.
Mi79 Mittlefehdt, D. W., and G. W. Wetherill. 1979. *Geochim. Cosmochim. Acta* **43**:201–206.
Mo67 Morgan, J. W., and J. F. Lovering. 1967. *Geochim. Comochim. Acta* **31**:1893–1909.

Table D-1 *(continued)*

Mo68 Morgan, J. W., and J. F. Lovering. 1968. *Talanta* **15**:1079–1095.
Na74 Nakamura, N. 1974. *Geochim. Cosmochim. Acta* **38**:757–775.
Ni74 Nichiporuk, W., and C. B. Moore. 1974. *Geochim. Cosmochim. Acta* **38**:1691–1701.
Pa78 Palme, H., et al. 1978. *Proc. Lunar Planet. Sci. Conf. 9th*, pp. 25–57.
Pa81 Palme, H., and W. Rammensee. 1981. *Earth Planet. Sci. Lett.* **55**:356–362.
Re60 Reed, G. W., et al. 1960. *Geochim. Cosmochim. Acta* **20**:122–140.
Re66 Reed, G. W., and R. D. Allen, Jr. 1966. *Geochim. Cosmochim. Acta* **30**:779–800.
Re67 Reed, G. W., and S. Jovanovic. 1967. *J. Geophys. Res.* **72**:2219–2228.
Ro82 Robert, F., and S. Epstein. 1982. *Geochim. Cosmochim. Acta* **46**:81–95.
Sc64 Schmitt, R. A., et al. 1964. *Geochim. Cosmochim. Acta* **28**:67–86.
Sc72 Schmitt, R. A., et al. 1972. *Meteoritics* **7**:131–213.
Sh79 Shima, M. 1969. *Geochim. Cosmochim. Acta* **43**:353–362.
Sm64 Smales, A. A., et al. 1964. *Geochim. Cosmochim. Acta* **28**:209–233.
Sm77 Smith, C. L., et al. 1977. *Geochim. Cosmochim. Acta* **41**:676–681.
Ta76 Tatsumoto, M., et al. 1976. *Geochim. Cosmochim. Acta* **40**:617–634.
Ta78 Takahashi, H., et al. 1978. *Geochim. Cosmochim. Acta* **42**:97–106.
Wa74 Wänke, H., et al. 1974. *Earth Planet. Sci. Lett.* **23**:1–7.
Wi69 Wiik, H. B. 1969. *Commun. Phys.-Math.* (Helsinki) **34**:135–145.

APPENDIX E

Radionuclides Used to Date Meteoritic Events

Table E-1 lists the long-lived and extinct radionuclides whose decay reactions are used to date meteoritic events, their stable daughter nuclides that exist in measurable abundances, their half-lives, and their decay constants.

Table E-1
Properties of radionuclides used to date meteoritic events

Parent	Measurable stable daughter(s)	Half-life $T_{1/2}$	Decay constant (yr^{-1})
Long-lived radionuclides:			
^{40}K	^{40}Ar, ^{40}Ca	1.25 Gyr	5.55×10^{-10}
^{87}Rb	^{87}Sr	48.8 Gyr	1.42×10^{-11}
^{147}Sm	^{143}Nd	106. Gyr	6.54×10^{-12}
^{187}Re	^{187}Os	~50. Gyr	$\sim 1.4 \times 10^{-11}$
^{232}Th	^{208}Pb, ^{4}He	14.0 Gyr	4.95×10^{-11}
^{235}U	^{207}Pb, ^{4}He	0.704 Gyr	9.85×10^{-10}
^{238}U	^{206}Pb, ^{4}He	4.47 Gyr	1.55×10^{-10}
Extinct radionuclides:			
^{26}Al	^{26}Mg	0.72 Myr	9.6×10^{-7}
^{107}Pd	^{107}Ag	6.5 Myr	1.07×10^{-7}
^{129}I	^{129}Xe	16. Myr	4.3×10^{-8}
^{244}Pu	$^{131-136}Xe$*	82. Myr	8.5×10^{-9}

Source: Adapted from T. Kirsten, in *The Origin of the Solar System*, ed. S. F. Dermott, p. 267. Wiley, 1978.
* Many other fission products also are produced.

APPENDIX F

Calculation of Equilibrium Relationships in the Solar Nebula

Insight into the fractionations observed in chondritic meteorites can result from the comparison of elemental abundances with those expected if stable solid phases were gained or lost from a cooling solar nebula. The solid phases that form by equilibrium processes in the solar nebula can be determined by following the principles of chemical thermodynamics. Consider the simple chemical reaction

$$a\,A + b\,B = c\,C + d\,D \tag{F-1}$$

in which a moles of substance A react with b moles of substance B to produce c moles of substance C and d moles of substance D. At any temperature we can write an **equilibrium constant** K for this reaction:

$$K = \frac{C^c D^d}{A^a B^b} \tag{F-2}$$

where (if the substances behave ideally) A, B, C, and D represent pressures for gaseous substances or concentrations for solid or liquid[1] substances. If, as is generally true, the substances behave nonideally, then a corrected pressure called **fugacity** is used for gases, and a corrected concentration called **activity** is used for solids and liquids.

Thermochemical data are commonly tabulated in terms of various functions. One of these, the Gibbs free energy G, is related to the equilibrium constant K as

$$\Delta G = -RT \ln K \tag{F-3}$$

where T is the absolute temperature, R is the gas constant, and the Δ in front of the G means "the change in" G during the reaction as written. Gibbs-free-energy data are commonly tabulated as the free energies of formation ΔG_f from the elements in their standard states (their states at a temperature

[1] No liquids form as stable phases in a low mass solar nebula having $p_{H_2} < 10^{-2}$ atm.

Table G-1 *(continued)*

Element	50-percent condensation temperature (K) 10^{-4} atm	10^{-5} atm	10^{-6} atm	References
Lu	1597	——	——	Bo80
Hf	1652	——	——	Gr74a
Ta	1550	——	——	Gr74a
W	1802	——	1631	Wa81; see also Gr74a, Pa76, Fe84
Re	1819	——	1669	Wa81; see also Gr74a, Pa76, Fe84
Os	1814	——	1666	Wa81; see also Gr74a, Pa76, Fe84
Ir	1610	——	1464	Wa81; see also Pa76, Fe84
Pt	1411	——	1278	Wa81; see also Pa76, Fe84
Au	1225	——	1074	Wa79
Hg	——	——	——	——
Tl	——	428	——	Gr74a
Pb	——	496	——	Gr74a
Bi	——	451	——	Gr74a
Th	1545	——	——	Bo81; see also Gr74a
U	1420	——	——	Bo81; see also Gr74a
Pu	1520	——	——	Bo81; see also Gr74a
Cm	1530	——	——	Bo81

References:

An76 Anders, E., et al. 1976. *Geochim. Cosmochim. Acta* **40**:1131.
Bo80 Boynton, W. V. 1980. Personal communication.
Bo81 Boynton, W. V. 1981. Personal communication.
Fe80 Fegley, B. 1980. Personal communication.
Fe84 Fegley, B., and H. Palme. 1984. *Earth Planet. Sci. Lett.* (submitted).
Gr74a Grossman, L., and J. W. Larimer. 1974. *Rev. Geophys. Space Phys.* **12**:71.
Gr74b Grossman, L., and E. Olsen. 1974. *Geochim. Cosmochim. Acta* **38**:173.
Ka85 Kallemeyn, G. W. and J. T. Wasson. 1985. *Rev. Geophys. Space Phys.* (submitted).
La84 Larimer, J. W. 1984. Personal communication.
Pa76 Palme, H., and F. Wlotzka. 1976. *Earth Planet. Sci. Lett.* **33**:45.
Se78 Sears, D. 1978. *Earth Planet. Sci. Lett.* **41**:128.
Wa77 Wai, C. M., and J. T. Wasson. 1977. *Earth Planet. Sci. Lett.* **36**:1.
Wa78a Wai, C. M., et al. 1978. *Lunar Planet. Sci.* **9**:1193.
Wa78b Wasson, J. T. 1978. In *Protostars and Planets*, ed. T. Gehrels, pp. 478–501. University of Arizona Press.
Wa79 Wai, C. M., and J. T. Wasson. 1979. *Nature* **282**:790.
Wa81 Wai, C. M. 1981. Personal communication.

APPENDIX H

Rudiments of Celestial Mechanics

The motion of a body in orbit about another body describes an ellipse. The properties of an ellipse are summarized in Figure H-1*a*. The long axis is called the major axis, the short axis the minor axis. The most-commonly-used property of an orbital ellipse is one-half of the major axis, called the **semimajor axis** and generally represented by the symbol a. One-half of the minor axis is called the **semiminor axis** and represented by b.

As also shown in Figure H-1*a*, an ellipse has two foci. The sum of the distance from any point on the perimeter to each of the foci is $2a$; thus the distance from either focus to the outer end of a semiminor axis is a. From this fact and the relation between the sides of a right triangle, one can readily show that the distance f from the center to either focus is given by the relationship $f = (a^2 - b^2)^{1/2}$.

The eccentricity e is a common measure of the shape of the ellipse; it is defined by $e = f/a$ and can have any value between 0 and 1. If $e = 0$, the ellipse is a circle; if $e = 1$, the ellipse is a line segment.

The typical orbit relevant to this text is described by a smaller body in orbit about a much larger body — for example, a planet or meteoroid in orbit about the Sun. In such a case, the larger body occupies one focus of the elliptical orbit. An elliptical heliocentric orbit is shown in Figure H-1*b*. Two other quantities are defined to facilitate the discussion of such an orbit: the greatest distance from the Sun is called the **aphelion** Q, and the least distance from the Sun is called the **perihelion** q. Note that these distances combine to yield the major axis, so that $Q + q = 2a$. For the general case of an orbit about any massive object, these quantities are given the generic names apoapsis (still represented by Q) and periapsis (q). For a satellite of the Earth, the relevant names are apogee (Q) and perigee (q).

A body in heliocentric orbit moves fastest near perihelion, slowest near aphelion. This observation was first put into quantitative terms by Kepler, whose second law states that "a line between the planet and the Sun sweeps out equal areas in equal amounts of time." Thus, if the aphelion distance is 3 times greater than the perihelion distance, an object's orbital velocity will be 3 times greater at perihelion than at aphelion.

For a small object in a circular orbit about a large body, the orbital velocity v can be derived by equating the gravitational force $F_g = GMm/a^2$ with the centrifugal force $F_c = mv^2/a$, where M is the mass of the large body, m is the mass of the small body, and G is the universal gravitational constant. This equation yields the result

$$v = \left(\frac{GM}{a}\right)^{1/2} \qquad \text{(H-1)}$$

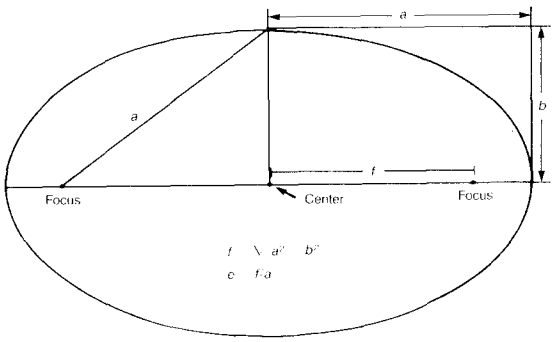

a. Properties of an ellipse

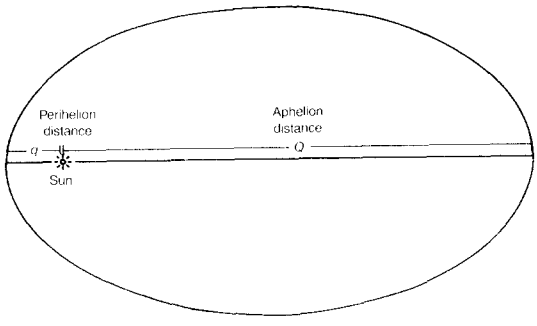

b. Elliptical heliocentric orbit

Figure H-1. *(a)* **Sketch of an ellipse, showing the symbols representing the main parameters: semimajor axis** a**, semiminor axis** b**, two foci each a distance** f **from the center, and the eccentricity** e**.** *(b)* **In an elliptical heliocentric orbit, the Sun occupies one focus. The greatest distance from the Sun is called the aphelion** Q**, the shortest distance from the Sun the perihelion** q**. Together** Q **and** q **comprise the major axis of the ellipse.**

Equation H-1 also is valid for the *mean* orbital velocity of an object in an elliptical orbit. The velocity at any point in an elliptical orbit is given by

$$v = \left[GM\left(\frac{1}{r} - \frac{1}{2a}\right)\right]^{1/2} \tag{H-2}$$

where r is the distance separating the small and large bodies.

The period p of a body in an elliptical orbit is given by $p = 2\pi a/v$, where v is the mean velocity. Substituting the value of v given by Equation H-1, we obtain

$$p = \frac{2\pi a^{1.5}}{G^{0.5}M^{0.5}} = Ka^{1.5} \tag{H-3}$$

In the final part of Equation H-3, the constant terms are combined to give a single constant K. For heliocentric orbits, K is unity if p is expressed in yr and a in AU. If the mass of the smaller object is not negligible relative to that of the more massive body, then one must substitute $(M + m)$ for M in Equation H-3. The relationship described by Equation H-3 is Kepler's third law. (His first law states that planetary motions describe elliptical orbits.)

The orbits of the planets are nearly coplanar with that of the Earth, but the typical angles between the orbital planes of asteroids and that of the Earth are about 10°, and the angles between the planes of long-period comets and that of the Earth can have any value between 0° and 180°.

This angle between the two orbital planes is called the **inclination** i. It is illustrated in Figure H-2. The most common reference plane is the plane of the Earth's orbit (the **ecliptic plane**), but for some purposes the mean plane of the solar system (essentially the same as the plane of Jupiter's orbit) is more useful.

Although the definition of inclination is commonly illustrated as the angle between planes as shown on a diagram such as Figure H-2, this representation is ambiguous because either of two angles (that sum to 180°) could be chosen. A more-exact definition of the inclination is the angle between the north polar vectors of the orbits, where the north polar vector is the perpendicular direction in which the thumb of the right hand points when the fingers point in the direction of an object's motion in its orbit.

In order for a meteoroid (or asteroid or comet) to enter the Earth's atmosphere, the meteoroid's orbit must intersect the orbit of the Earth. If the meteoroid's orbit is inclined to that of the Earth, the intersection can occur only along the **line of nodes** defined by the intersection of the two orbital planes (see Figure H-2). If the meteoroid is in a typical orbit having a moderate eccentricity, there normally can be only one point at which the

Metallic iron in a typical chondrite will show up as shiny millimeter-sized spots on a flat surface produced by grinding. The combination of shiny metallic spots, a weak magnetic attraction, and a density of at least 3.3 $g \cdot cm^{-3}$ is strong evidence that a rock is a meteorite.

Human-produced iron is the material most likely to masquerade as an iron meteorite. In many cases, artificial iron has shapes (such as straight edges or 90° corners) distinctly different from those of meteorites (see Chapter II). Nickel, which is present at levels of at least 40 mg/g (4 wt%) in every iron meteorite, is present in human-made iron only as an uncommon additive — in stainless steel, for example. Stainless steel generally contains more chromium than nickel, however, whereas chromium in iron meteorites virtually never is present at levels as great as 1 mg/g. Artificial iron commonly contains other alloying elements such as vanadium, manganese, silicon, or carbon that are present at very low levels in meteoritic iron.

An iron meteorite can almost always be recognized by the texture revealed by etching a polished surface. In particular, most irons show the Widmanstätten pattern illustrated in Figures II-6, II-7, and II-8. This pattern is revealed by etching a finely polished surface with nital, a 2-percent solution of concentrated nitric acid in ethanol. Care is needed because this acid interacts strongly with human skin!

The external morphology of a meteorite is commonly characteristic. The wavelike surface seen on the Cabin Creek iron (Figure I-3) is found on many (but not all) iron and in a more subdued "thumbprinted" form on many stones. Some morphologies are virtually never found. For example, it appears (based on samples sent to me for identification) that many persons believe meteorites to have frothy, porous, or slaggy textures; in fact, meteorites are invariably compact, with no visually recognizable porosity.

Almost every freshly fallen meteorite has a dark fusion crust covering the surface. The blackness of the crust contrasts with the light gray of the interior of many stones. In some plagioclase-rich meteorites, the fusion crust is quite shiny (see Figure II-5). Unfortunately, the crust becomes the reddish color of iron rust within a few years; thus, in most cases, the color of meteorite finds is rather similar to those of other local rocks. Partly because of this, new stony meteorite finds are rarely recognized in rocky areas. It is not a coincidence that most meteorite finds in the U.S. are recovered from the fine, rock-free soil of the western plains.

If you have an object having properties indicating that it may be a meteorite, the best way to obtain confirmation is to send a small, walnut-size fragment to a major meteorite collection. You can send it to me at UCLA, Los Angeles, CA 90024, for free examination. The same service is offered in the U.S. by the American Museum of Natural History, New York, NY 10024; Arizona State University, Tempe, AZ 85281; the Field Museum of Natural History, Chicago, Il 60605; the Smithsonian Institution, Washington, DC 20560; and the University of New Mexico, Albuquerque, NM 87131. Other important world locations offering this service are the Geological Survey of Canada, Ottawa K1A 0E8 Ontario, Canada; the British Museum (Natural History), London SW7 5BD, England; and Muséum Histoire Naturelle, Paris 75005, France; the Naturhistorisches Museum, Vienna A-1014, Austria; the Max Planck Institut für Chemie, Mainz D-6500, Federal Republic of Germany; the Western Australian Museum, Perth, WA 6000, Australia; and the national scientific or natural-history museums of many other countries.

One of the best ways to learn to recognize meteorites is to visit meteorite exhibits at museums. Note in particular the morphologies and colors of the finds, especially the stony-meteorite finds (irons are much easier to recognize).

If you should ever have the grand fortune to see a meteorite streak through the sky, the chief piece of information you should note is the exact direction in which it disappeared. Point to and fix in your mind a distant landmark that is in line with the end of the fireball's path, and then note exactly where you are standing.

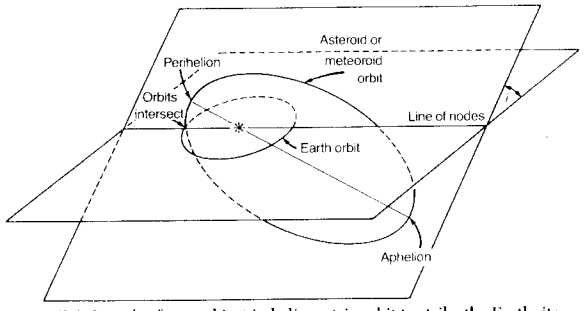

Figure H-2. In order for an object in heliocentric orbit to strike the Earth, its orbit must intersect that of the Earth. The angle between the planes of the two orbits is the inclination *i*. Intersection of the orbits can occur only along the line of nodes formed by the intersection of the orbital planes. Because of perturbations of the orbital elements by the planets, any particular Earth-crossing orbit is Earth-intersecting during only a small fraction of the time.

two orbits can intersect (the trivial exception occurs if the major axis of the meteoroid's orbit is perpendicular to the line of nodes). In most orbital passages, the meteoroid and the Earth do not reach the intersection point at the same time.

As a result primarily of gravitational perturbations by Jupiter, the orientation of a meteoroid's orbit undergoes significant changes on a time scale of 10 to 100 kyr. Although most objects in **Earth-crossing orbits** (those with $Q > 1$ AU and $q < 1$ AU) do not actually intersect the Earth's orbit, these changes in orientation cause the orbits to be intersecting a small fraction of the time. When one includes the effects of these long-distance perturbations, one finds that an Earth-crossing meteoroid (or larger object) about once each megayear makes a close approach to the Earth that causes a major change in the orbital parameters but leaves the object in an Earth-crossing orbit, because the object's new orbit must include the point where the close approach to the Earth occurred.

If an object is in an Earth-crossing orbit confined to the inner solar system ($Q < 4.5$ AU), it will not be able to come close enough to Jupiter to receive a major impulse. Numerical simulations show that the object will be removed from such an orbit after about 10 Myr. The most probable fates that await it are collision with the Earth, collision with Venus, or an orbital perturbation by one of these planets that makes it Jupiter-crossing and allows Jupiter to eject it from the solar system within about 100 kyr.

APPENDIX I

How to Recognize Meteorites

Conversations with both professional and lay persons reveal that they and I share a common fascination; when we take walks, we are continuously (though often subconsciously) visually examining the rocks along the trail for possible meteorites. I have never found a meteorite in this fashion, and less than 1 in 1000 persons who indulge in this habit will ever find a meteorite. It's fun nonetheless, and it is therefore useful to know what clues indicate that a strange rock might be a meteorite.

As discussed in some detail in Chapter II, most meteorites that are seen to fall are chondrites, the remainder being stony-irons and differentiated silicate-rich meteorites (~9 percent) and irons (~6 percent). About 85 percent of all meteorites contain at least 20 mg/g (2 wt%) metallic Ni–Fe and, because these metal-bearing meteorites are more resistant to weathering, the proportion of meteorite finds that are metal-bearing is at least 95 percent. Because metallic Fe–Ni is extremely rare among terrestrial rocks, the presence of such metal in a "rock" is the best indication that the rock is a meteorite.

A key question then is how can one most easily find out whether a rock contains metallic iron. Those with modern analytical equipment available will have no trouble showing that the metal is Fe–Ni; the most straightforward technique is to analyze suspicious minerals with the electron microprobe, a device that measures X rays emitted by the sample following its bombardment by electrons.

Those who do not have analytical facilities available can use a series of clues to tell them whether metallic Fe–Ni is present. Because of the high density of metal (~8 g · cm^{-3}), meteorites containing metal, with rare exceptions, have densities of at least 3.3 g · cm^{-3} (3.3 times the density of water), appreciably denser than other local rocks. The rare terrestrial rocks having densities greater than or equal to 3.3 g · cm^{-3} are generally iron ores such as hematite or magnetite. Density can be measured by weighing an object to determine the mass and dividing this by the volume, which can be determined by various techniques, the most accurate method is weighing the object again while suspended in a liquid such as water. The volume in cubic centimeters is numerically equal to the reduction in mass in grams that results from suspension in water.

Meteoritic metal responds to a magnet. If much metal is present, the magnet will cling to the rock; minor amounts of metal can be detected by hanging the magnet on a string and testing to see if the rock has enough attraction to cause the magnet to swing away from the vertical. Of course, human-produced metallic iron attracts a magnet equally strongly, and some iron ores such as magnetite also show an appreciable attraction.